# Development and regeneration of the retinotectal map in goldfish: a computational study

CORNELIUS WEBER[1], HELGE RITTER[2], JACK COWAN[3] AND KLAUS OBERMAYER[1]

[1] *Fachbereich Informatik, Technische Universität Berlin, Germany* (cweber@cs.tu-berlin.de)
[2] *Technische Fakultät, Neuroinformatik, Universität Bielefeld, Germany*
[3] *Department of Mathematics and Neurology, The University of Chicago, USA*

**CONTENTS**



**SUMMARY**

We present a simple computational model to study the interplay of activity-dependent and intrinsic processes thought to be involved in the formation of topographic neural projections. Our model consists of two input layers which project to one target layer. The connections between layers are described by a set of synaptic weights. These weights develop according to three interacting developmental rules: (i) an intrinsic fibre–target interaction which generates chemospecific adhesion between afferent fibres and target cells; (ii) an intrinsic fibre–fibre interaction which generates mutual selective adhesion between the afferent fibres; and (iii) an activity-dependent fibre–fibre interaction which implements Hebbian learning. Additionally, constraints are imposed to keep synaptic weights finite. The model is applied to a set of eleven experiments on the regeneration of the retinotectal projection in goldfish. We find that the model is able to reproduce the outcome of an unprecedented range of experiments with the same set of model parameters, including details of the size of receptive and projective fields. We expect this mathematical framework to be a useful tool for the analysis of developmental processes in general.

## 1. INTRODUCTION

Topographic projections between layers of cells are a common structural feature in the central nervous system of many species. It has been hypothesized that those projections emerge not only because they serve a common computational goal but also because they are well adapted to a set of fairly universal developmental mechanisms. The fact that topographic projections are widespread and a robust phenomenon makes their genesis an important subject of investigation.

The retinotectal projection in lower vertebrates has been the system of choice for exploring topographic projections and their formation. During development, retina and tectum are formed before connections between them are established. Axons of retinal ganglion cells sprout at a time when both organs are still small and they grow from each eye via the optic nerves and tracts towards the anterior, contralateral tectum. When they reach their targets, fibres disperse across large areas of tectum but avoid regions too far from the proper termination site. Subsequently, their termination areas shrink and projective fields are confined to their topographically correct regions. Ganglion cells from the ventral, dorsal, nasal and temporal part of the retina finally project to the medial, lateral, caudal and rostral tectum, respectively. Because the retina grows at the ciliary margin while tectum grows at the caudal end, development involves a continuous reorganization of the topographic map.

When the optic nerve is sectioned, afferent axons develop growthcones and grow towards tectum even in adult goldfish. Axons are disordered in the optic nerve (Stuermer 1986) and—compared to normal development—terminal arbors refine in a more irregular fashion with multiunit receptive fields emerging temporarily (Stuermer 1988). Finally, a normal topographic projection is established, but an abnormal

structure of the tectal layers may persist after some experiments (Yoon 1975*b*).

Despite certain differences between development and regeneration the latter has been well investigated as a model system for the formation of topographic projections. Regeneration processes allow experiments to be performed on large adult animals and, therefore, allow easy experimental access. Consequently, there exists a large database of regeneration experiments (see, for example, Fraser & Perkel (1990); Friedman (1993) or the next section for a review). Because regeneration involves not only activity driven 'learning' but also intrinsic non-activity based sprouting and retraction of fibres such experiments can be used as a testbed for theories of neural development, where several mechanisms of differing nature interact. Under the assumption of 'approximate' universality of mechanisms, regeneration experiments should provide insight into the formation of neural projections in general.

In the past, there have been a handful of modelling approaches towards interacting mechanisms in topographic map formation. The goal was to: (i) characterize the nature of the individual mechanisms; (ii) to understand their interaction; and (iii) to serve as a guideline for further experiments. All models take into account the experimental finding that the mechanisms of regeneration try to fulfil two sometimes conflicting goals (Whitelaw & Cowan 1981) dubbed 'specificity' and 'plasticity'. In this context, specificity refers to the high precision with which retinal fibres connect both layers and plasticity refers to the ability of the projection to adapt even to drastic experimental manipulations of retinal and tectal tissue. So far, previous approaches have not been completely satisfying. The *marker induction* (Willshaw & von der Malsburg 1979) and *arrow* models (Overton & Arbib 1982), for example, postulate a fixed strength of fibre–tectum versus fibre–fibre interactions and discard activity driven processes. The *multiple constraint model* (Fraser & Perkel 1990) allows to fit the effect individual processes have on map-formation against the data, by changing the values of appropriate coupling constants. The model, however, makes no predictions about the time-course of development and about receptive and projective fields. The model of Friedman & Cowan (1990) allows predictions about the time-course but does not yet include all of the suggested mechanisms and has not yet been tested against all relevant experiments.

In this contribution we further develop the ansatz of Friedman & Cowan. We simplify the developmental mechanisms so that they are all linear with respect to the synaptic strengths, and we discard the effects of retinal fibre debris on tectum, which is an artifact of 'unclean' regeneration experiments. We extend their approach to the two-dimensional case, and we perform extensive numerical simulations to cover all experimental paradigms. Results of numerical simulations are analysed with respect to topography and to the size and the shape of receptive and projective fields. We demonstrate that there exists a parameter regime, where the outcome of all different experiments is predicted correctly. Due to the different goals pursued by the different developmental mechanisms, predictions may not be very robust for certain experimental paradigms, where these goals are in conflict. This is again in accordance with the literature, where a certain percentage of 'failures' and a certain 'brittleness' in the experimental outcome is reported. The results thus illustrate very well what kind of experiments may provide robust information about the nature of the underlying processes and what kind of experimental outcomes may be subject to uncontrollable details. We therefore expect this ansatz to be a useful tool to interpret and design new experiments not only in goldfish but in other species of current interest like the zebrafish (see Goodman & Shatz 1993 for a review).

The paper is divided into five parts. After a review of the relevant experiments and a brief discussion of previous computational approaches we describe our ansatz in § 3. This is followed by § 4, which contains the results, and by § 5 which concludes the paper with a discussion of our findings. For reason of consistency, we mostly restrict our discussion to experiments which have been performed in the goldfish system.

## 2. A REVIEW OF EXPERIMENTAL FINDINGS AND MODELS

### (*a*) *Experimental findings*

Many *in vivo* surgery experiments in the past have been designed to settle the question of which mechanisms play the dominant role in development. An old hypothesis—called the chemoaffinity hypothesis (Sperry 1943, 1963)—stated that afferent fibres specifically recognize their target location in tectum. This simple and straightforward hypothesis was supported by a set of regeneration experiments called 'translocation' and 'rotation'.

In these experiments, grafts of tissue were dissected from tectum and reimplanted after they have been either rotated around the vertical axis by 90° or 180°, after they have been inverted (Yoon 1973, 1975*b*) or after two of them have been exchanged (Hope *et al.* 1976). In general, the optic fibres found their original sites even on the rotated or translocated grafts, except when the exchanged grafts were small and close together in which case an undisturbed topographic map was formed. It was found that the displaced projection can shrink or expand towards intact areas (Hope *et al.* 1976). In order to rule out a decisive influence of previous innervation graft rotation experiments have been performed, albeit in the Xenopus system, where the initial projection was either completely scrambled (Hunt 1976) or lacking (Straznicky 1978). Again, the topographic map exhibited a rotated part.

Although initial experiments supported Sperry's ideas, other experiments were performed, whose outcomes stressed plasticity, i.e. the ability to override any specific markers for the sake of an undisturbed

topographic projection. Those regeneration experiments were called 'compression', 'expansion' and 'mismatch'.

When fibres from only half of the retina are deflected onto a tectum which has been denervated for at least 150 days (Schmidt 1978*a*) the final projection is expanded across the whole tectum and polarity as well as topography are preserved. When optic fibres from a whole eye are allowed to invade a half-tectum which has been denervated for 40 days (Yoon 1975*a*) a compressed topographic map with correct polarity is formed. In the mismatch experiment (Horder 1971) the temporal part of the retina and the caudal part of the tectum are removed such that the non-corresponding parts remain. The final projection is again topographic and polarity is preserved.

It seems as if the mechanisms underlying development serve the purposes: (i) reliable target finding; (ii) all retinal cells connect to tectal target cells; (iii) every tectal cell receives retinal input; and (iv) preservation of topography. Directional information seems more important than positional information. In normal development all goals are *d'accord*.

How can a mechanism lead axons to specified target areas and at the same time allow such large scale corrections like in the expansion experiment? Gierer (1983) modified the chemospecificity hypothesis towards the idea of a graded distribution of chemical markers which may provide global specificity and local polarity information rather than enforce a one–to–one correspondence between retinal fibres and tectal sites. Following up on this hypothesis the distribution of chemical markers has been accessed through *in vitro* studies like the striped carpet essay (Walter *et al.* 1987; Stahl *et al.* 1990; Vielmetter *et al.* 1991; Baier & Bonhoeffer 1992). More recently, some gradedly distributed markers have been found in retina and tectum like RAGS and ELF-1 ligands which decrease linearly from caudal towards rostral tectum (Drescher *et al.* 1995; Cheng *et al.* 1995) and Mek4 receptor which is distributed in the retina in a temporal to nasal gradient (Cheng *et al.* 1995). A protein with a step-function like distribution has not been proved, but the TRAP protein shows itself to be preferentially distributed on the temporal retina, possibly in a step-like distribution (McLoon 1991). See Holt & Harris (1993) for a review.

What is the factor mediating plasticity? It has been proposed that electrical activity may be the factor, which underlies plasticity and which ensures topography under abnormal experimental conditions. Activity dependent mechanisms can be demonstrated when fibres from both eyes are made to grow onto one tectum. Ocular dominance patches emerge (Meyer 1979*b*), but their formation is suppressed, when retinal activity is blocked in both eyes (Meyer 1982). Note that the projections from two nasal half retinae expand across the whole tectum while forming stripes (Fawcett & Willshaw 1982). The prevailing view is that pre- and post-synaptic cells connect when simultaneously active. Due to correlated activity in the retina—as is usually assumed—this

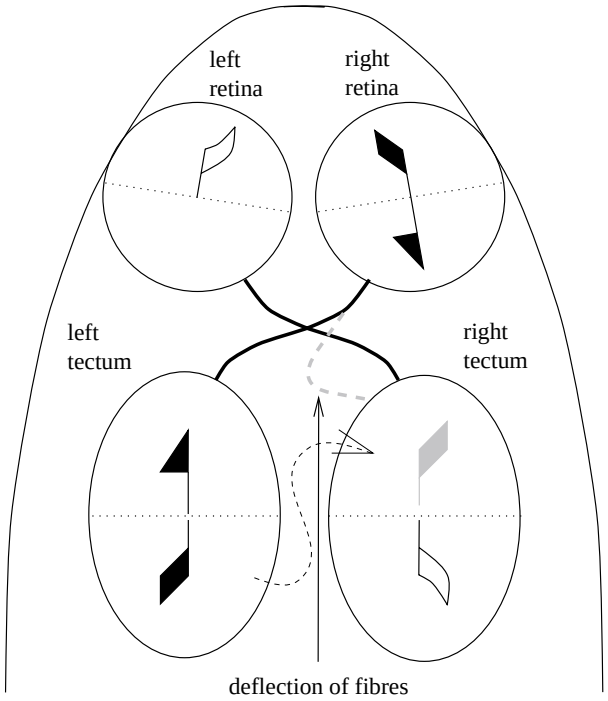


Figure 1. Cartoon of the polarity reversal experiment. A section in top view of the goldfish is shown with both retinae and tecta. Matching arrows show how corresponding regions are normally connected, via the optic nerve (thick lines). In the experiment, the anterior right tectum is denervated (the temporal left retina does not project). A part of the optic nerve which hosts fibres which project to the posterior left tectum (dashed, grey line) is deflected to the denervated area. The thin, curved line summarizes this displacement. The grey arrow-tail in the anterior right tectum shows the polarity of this mismatched projection after regeneration.

Hebbian-type mechanism (Hebb 1949) bundles retinal fibres from nearby retinal sites within the corresponding eye and thus assists topography. Blocking of electrical activity by TTX (Olson & Meyer 1994) as well as impeding correlated firing through stroboscopic light (Cook & Rankin 1986; Schmidt & Buzzard 1993) prevents the refinement of projective fields.

Activity, however, cannot be the only mechanism mediating plasticity, because expansion, for example, occurs under TTX-blockade (Olson & Meyer 1994). Other experiments provide direct evidence for an interaction between retinal fibres, which is intrinsic rather than activity dependent. A repulsion of temporal retinal growth cones occurs at contact with nasal retinal axons *in vitro* (Raper & Grunewald 1990). Experiments show that temporal retinal fibres are attracted to those locations in tectum which are innervated by fibres from mirror-symmetrically corresponding locations in the contralateral retina. When they are deflected into an intact projection they are confined to the rostral tectum, but when there is an already expanded half-retinal contralateral projection then they expand correspondingly (Schmidt 1978*a*).

The most outstanding example for intrinsic fibre–

Table 1. *Experiments and mechanisms*

((c) indicates that the way the mechanism acts is in conflict with the experimental outcome. Mechanisms marked with (√) are consistent with the outcome. The fibre–tectum interaction is listed for two competing model assumptions, namely absolute positional specificity, left, and graded cues, right.)

| | interaction | | | |
|---|---|---|---|---|
| | fibre–tectum | | intrinsic | activity |
| experiment | specific | graded | fibre–fibre | fibre–fibre |
| rotation | √ | √ | c | c |
| translocation | √ | √ | c | c |
| expansion | c | √ | √ | √ |
| compression | c | √ | √ | √ |
| mismatch | c | √ | √ | √ |
| half-retina into normal map | √ | √ | √ | √ |
| Meyer-polarity-reversal | c | c | √ | √ |
| two retinae with TTX | √ | √ | √ | √ |
| two half-retinae | c | √ | c | √ |

fibre interaction is the polarity reversal experiment (Meyer 1979*a*). In this experiment the innervation of one anterior tectal half is permanently removed (upper right tectum in figure 1). At the same time a select fraction of ipsilateral nasal optic fibres, those which normally innervate the posterior contralateral (left) tectum are deflected into the anterior half. Thus, deflected fibres grow into an inappropriate but denervated region of a tectum in which the appropriate target region is already occupied. The final projection is observed to be topographic, albeit with a reversed polarity: in the figure, the dashed arrow shows posteriorly, such that the tip (where fibres come from the middle of the right retina) touches the tip of the open arrow (where fibres come from the middle of the left retina). This experiment has to be compared with the mismatch experiment (Horder 1971) which is similar except that the posterior half tectum is removed and thus there is no influence of normal posterior innervation. In this case a map with correct polarity was formed. The similarity of the surgery at both experiments and the fact that deflected fibres were still oriented normally at the insertion point in the polarity reversal experiment (Meyer 1979*a*) rules out a decisive influence of the organization of the retinal fibre bundle. Thus the reversal of polarity in Meyer's experiment provides evidence for a highly selective interaction between fibres which originate from corresponding regions of different eyes.

Table 1 summarizes experiments and putative mechanisms. Mechanisms act in concert in some of the experiments but may try to fulfil conflicting goals in others. Under the assumption of one dominant mechanism, the experimental findings in table 1 are contradictory. Any reasoning must therefore involve several mechanisms and their interaction. This situation calls for a modelling approach to complement experiments.

### (*b*) *Previous modelling approaches*

In the past, there have been a handful of modelling approaches towards interacting mechanisms in topographic map formation with the goal to: (i) characterize the nature of the individual mechanisms; (ii) to understand their interaction; and (iii) to serve as a guideline for further experiments. We will shortly describe a selection of models which are powerful in describing the retinotectal projection and/or which have contributed to our model.

The *(gradient) arrow model* (Hope *et al.* 1976) was designed to reformulate the chemospecificity hypothesis. Only one mechanism, the fibre–tectum interaction was implemented to give two retinal fibres information about the correctness of their *relative* positions on tectum and interchange them if appropriate. It explained the rotation experiment but failed at translocation which demonstrated that by small steps only, fibres are not able to find displaced targets. The following *extended branch arrow model* (Overton & Arbib 1982) combined in an additive fashion three interactions to calculate the movement of retinal branches on tectal surface: a fibre–fibre interaction, a fibre–tectum interaction and a restraining influence by tectal and graft boundaries. The goal was to explain a wide body of experiments and the model described expansion and compression well. Rotation and translocation, however, showed disorder and double nasal expansion did not predict the ocular dominance patches seen in experiments.

The *marker induction model* (Willshaw & von der Malsburg 1979) also assumes specific chemical markers. It states that markers are not innate but are induced by retinal fibres which innervate a given tectal site and by a following diffusion process. Synapses grow with respect to common molecules of a retinal fibre with a tectal site and thus preserve neighbourhood, a mechanism dubbed the molecular analogue of the Hebb (1949) rule.

Without the use of activity, the model explains rotation, translocation, expansion, compression and expansion of two temporal half retinae without ocular dominance patches. The nice outcome of the rotation experiment demonstrates the suitability of modifiable synapses for this modelling approach. As this model resolutely assumes there to be no innate tectal marker it cannot explain initial generation: there must be further cues which determine the polarity of the normal projection.

The *multiple constraint model* (Fraser & Perkel 1990) for the first time combines four mechanisms, position-independent induction of growth, fibre–tectum interactions, activity dependent fibre–fibre interactions and a competition of fibres for tectal space. Every interaction is described by a cost function which depends on the arrangement of fibres across tectal cells and which additively contributes to the total cost. Note, that one retinal cell makes connections to only one tectal site, i.e. the effect of extended retinal arbors is not considered and the development of receptive and projective fields is outside the current scope of the model. Fraser assumes that the developmental processes act to lower the total cost until the global minimum is reached, and supplies a random walk minimization procedure. The model nicely illustrates the cooperation and competition of the differing mechanisms for the different experimental paradigms. Given biologically plausible cost functions the model can explain expansion, compression, rotation and ocular dominance patches. Unfortunately, the authors do not point out the model's weaknesses: thus, a simulation of the translocation experiment is missing. Translocation is difficult to achieve—as has been shown by the *arrow model* (Hope *et al.* 1976)—when fibres can only make small steps.

The model by Whitelaw & Cowan (1981) describes topographic map formation as the interplay between activity driven Hebbian learning modulated in a multiplicative way by a fibre–tectum interaction due to chemical markers. In its original form it did not contain an intrinsic fibre–fibre term and was not able to account for the corresponding effects. The model was later extended by Friedman (1993) to incorporate intrinsic fibre–fibre interactions as well as the effect of the previous innervation observed in some of the older regeneration experiments. In principle, the Friedman–Cowan approach should be able to account for all the relevant experiments because it incorporates all the relevant mechanisms. However, no single parameter regime has yet been described for which all experiments, e.g. polarity reversal *and* translocation, are predicted correctly. The reason why such a model lacks consistency is its complexity: more than eight parameters plus the interaction widths balance the mechanisms which are nonlinear as well as time dependent.

In summary, previous modelling approaches are incomplete, because they either do not take into account all relevant mechanisms or they are not able to predict the outcome of all relevant experiments for one set of parameter values. Some of the modelling approaches are too complex, like the Friedman–Cowan approach. Other approaches are too simple, like the *multiple constraint model*, and do not include receptive and projective fields. In the following, we will simplify and extend the Friedman–Cowan (Whitelaw & Cowan 1981; Friedman & Cowan 1990, 1991) formulation, which seems to be the most promising approach towards a coherent mathematical framework of intrinsic and activity driven development.

## 3. MODEL AND IMPLEMENTATION

### (*a*) *Overview*

The following mathematical description is based on the Whitelaw & Cowan (1981) formulation. We describe the connectivity pattern between retinal and tectal sites by effective connection strengths, which lumps the number of synapses and the synaptic weights into one quantity, an effective connection strength. This simplification is made for the reason of computational efficiency.

In principle, numbers and weights can be separated and processes of sprouting/retraction versus synaptic weight may be treated separately.

Motivated by the experimental results reviewed in the last section we consider three mechanisms of interaction: (i) intrinsic fibre–tectum interaction; (ii) intrinsic fibre–fibre interaction; (iii) activity dependent fibre–fibre interaction.

Additionally, we consider five unspecific mechanisms or constraints: (i) an overall unspecific induction of connection strengths, (ii) a decay term proportional to a function of the total strength assigned to all fibres from one retinal location, (iv) a decay term proportional to a function of the total strength assigned to all fibres which connect to one tectal cell, (v) a decay term proportional to the synaptic weight and (vi) a lower bound of synapse strength at zero.

Unspecific growth of retinal fibres to somewhere in tectum underlies every experiment and is a fundamental assumption. The restriction to positive synaptic strengths reflects the involvement of one cell type only, namely the retinal ganglion cells. There is evidence for an approximate conservation of total synapse number (Olson & Meyer 1994), however, the exact form of the constraint is to some extent arbitrary and has to be fitted against data.

### (*b*) *Mathematical formulation*

Our model (figure 2) consists of two input layers which correspond to the retinae of both eyes and one output layer which corresponds to either the right or the left tectum. The second retina takes part only at those regeneration experiments which may result in binocularly innervated tectal areas. The connections between eyes and tectum are described by synaptic weights $S_{E,\boldsymbol{\alpha},\boldsymbol{x}}$, where $E$ denotes the retina (left or right), $\boldsymbol{\alpha}$ the retinal location and $\boldsymbol{x}$ the location on the tectum. Input and output layers are implemented either as two-dimensional square-shaped grids of

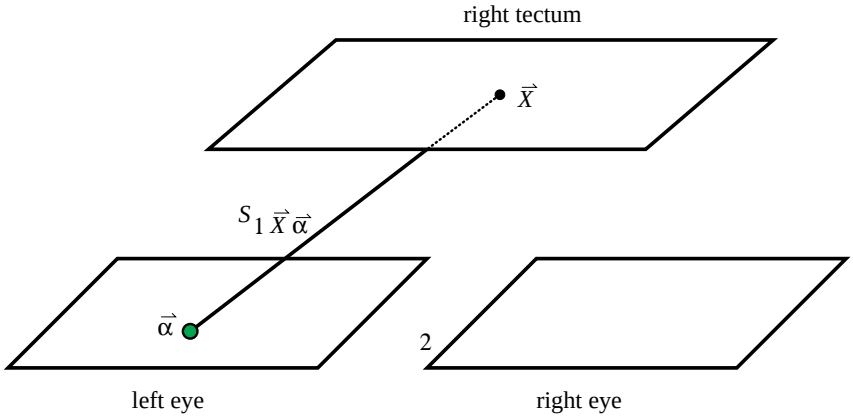


Figure 2. Cartoon of the computational model. Every cell in the retina is labelled by its retinal location $\boldsymbol{\alpha}$, every cell in tectum by its tectal location $\boldsymbol{x}$. $S_{E\boldsymbol{\alpha}\boldsymbol{x}}$ denote the connection strengths.

units, where each unit represents a cluster of cells, or as one-dimensional rows, if computational demands call for a simplified one-dimensional version.

Development of $S_{E,\boldsymbol{\alpha},\boldsymbol{x}}$ is described by the differential equation:

$$\frac{\mathrm{d}}{\mathrm{d}t}S_{E\boldsymbol{\alpha}\boldsymbol{x}} = N + aA_{\boldsymbol{\alpha}\boldsymbol{x}} + f^{\mathrm{int}}F^{\mathrm{int}}_{\boldsymbol{\alpha}\boldsymbol{x}}(\boldsymbol{S}) + f^{\mathrm{act}}F^{\mathrm{act}}_{E\boldsymbol{\alpha}\boldsymbol{x}}(\boldsymbol{S}) - c^{\mathrm{tec}}C^{\mathrm{tec}}_{\boldsymbol{x}}(\boldsymbol{S}) - c^{\mathrm{ret}}C^{\mathrm{ret}}_{E\boldsymbol{\alpha}}(\boldsymbol{S}). \quad (1)$$

Equation (1) is linear in $S$ in the sense, that all terms of the sum which depend on $S$ scale proportional to the magnitude of the $S$ values. Connection strengths would thus indefinitely increase in magnitude without an additional constraint. Therefore, connection strengths are kept positive by a hard limit at zero. We show in the appendix that growth underlying this equation searches for a minimum in an energy space which is confined by this limit.

Let us briefly discuss the different expressions on the right-hand side of equation (1). The quantity $A_{\boldsymbol{\alpha}\boldsymbol{x}}$ denotes the fibre–tectum interaction, which is chosen to be independent of the synaptic weights,

$$A_{\boldsymbol{\alpha}\boldsymbol{x}} = \tfrac{1}{4}((\mathbf{1}-\tilde{\alpha})\tilde{x} + \tilde{\alpha}(\mathbf{1}-\tilde{x})). \quad (2)$$

$\tilde{\alpha}$ and $\tilde{x}$ denote retinal and tectal locations, respectively, both scaled such that their vector components range from 0–1 which results in $A_{\boldsymbol{\alpha}\boldsymbol{x}}$ ranging from 0–1 in its amplitude. Two markers, their graded concentrations described by $(\mathbf{1}-\tilde{\alpha})$ and $\tilde{\alpha}$ in the retina interact with tectal markers of concentrations $\tilde{x}$ and $(\mathbf{1}-\tilde{x})$, respectively. Such marker distributions are the stationary result of a diffusion of markers into the tectum which have a fixed concentration at the borders. The interaction is multiplicative, thus proportional to the concentration of each of these substances. Both axes of retinal and tectal surface are labelled this way. The resulting function is of intermediate specificity in the sense that there are no large changes on a small area, and the strength of this convex function falls more rapidly the larger the distance is to the appropriate target area. Other functions, which were tested for the computationally less demanding one-dimensional model, include an even less specific step-function,

$$A^{\mathrm{step}}_{\alpha'x'} = \frac{1}{1+\mathrm{e}^{\gamma(\alpha'-0.5)}}\frac{1}{1+\mathrm{e}^{\gamma(x'-0.5)}}, \quad (3)$$

smoothed by a bias parameter $\gamma$ in which $\alpha'$ and $x'$ denote the (one-dimensional) retinal and tectal positions which are normalized to the interval $[0,1]$, and a highly specific Lorentz-type function,

$$A^{\mathrm{point}}_{\boldsymbol{\alpha}\boldsymbol{x}} = \frac{1}{|\boldsymbol{x}-\boldsymbol{x}^*(\boldsymbol{\alpha})|+1}, \quad (4)$$

in which $\boldsymbol{x}^*(\boldsymbol{\alpha})$ denotes the topographically correct position of a retinal axon at position $\boldsymbol{\alpha}$ on the tectal sheet.

Evidence for similar markers has recently been found in the retinotectal system. The ligand ELF-1 in the tectum and its receptor Mek4 in the retina (Cheng *et al.* 1995), for example, constitutes a possible molecular pair which could provide polarity information by a graded distribution along the anterior–posterior axis. Other markers like RAGS (Drescher 1995) and Sek (Cheng *et al.* 1995) are further candidates for gradients along the anterior–posterior axis.

A candidate for a stepfunction-like distributed marker is the *temporal retinal axon protein* found by McLoon (1991). No candidates have yet been found for a highly specific interaction similar to equation (4). It was, however, included in some of the numerical simulations to demonstrate its impact on map formation, because it is the most straightforward implementation of Sperry's (1943, 1963) chemospecificity hypothesis.

The intrinsic fibre–fibre interaction $F^{\mathrm{int}}_{\boldsymbol{\alpha}\boldsymbol{x}}$ is described by the expression

$$F^{\mathrm{int}}_{\boldsymbol{\alpha}\boldsymbol{x}}(\boldsymbol{S}) = \sum_{D}^{\mathrm{eyes}}\sum_{\boldsymbol{\beta},\boldsymbol{y}} S_{D\boldsymbol{\beta}\boldsymbol{y}}\, g(|\boldsymbol{\beta}-\boldsymbol{\alpha}|,\sigma^{\mathrm{int}}_{\mathrm{ret}}) \times g(|\boldsymbol{y}-\boldsymbol{x}|,\sigma^{\mathrm{int}}_{\mathrm{tec}}) - \tfrac{1}{2}S_{D\boldsymbol{x}\boldsymbol{\alpha}}, \quad (5)$$

in which

$$g(|\boldsymbol{r}|,\sigma) = n\exp(-|\boldsymbol{r}|^2/\sigma^2), \quad (6)$$

denotes a normalized Gaussian function. $|\boldsymbol{r}|$ denotes the length of the vector $\boldsymbol{r}$ and $n$ is a normalization

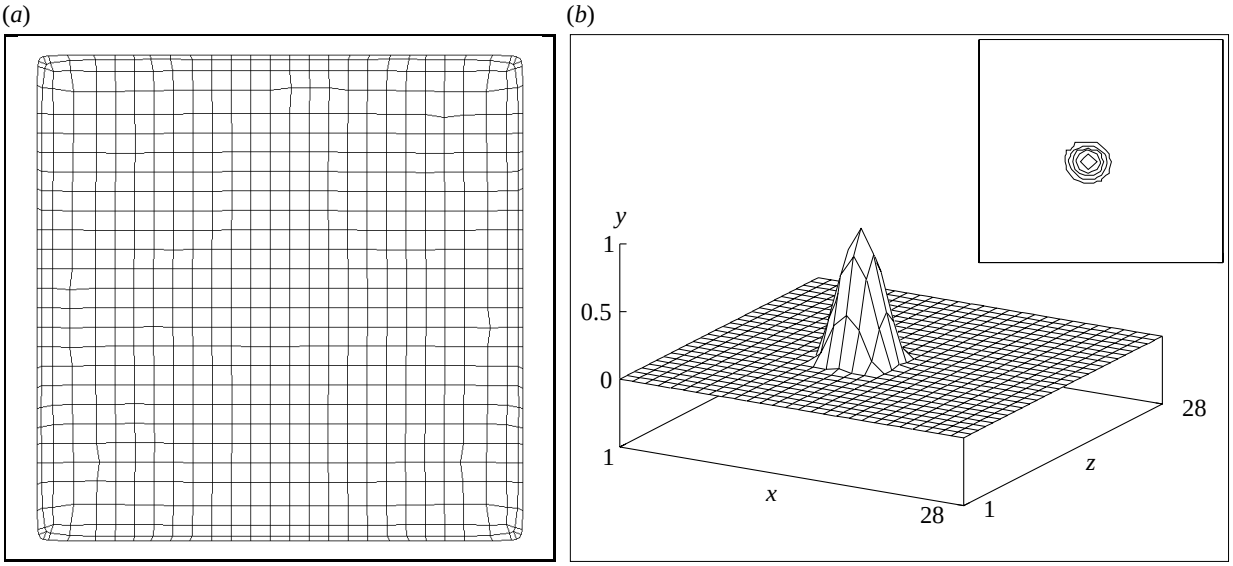


Figure 3. (*a*) Topographic map between retina and tectum after 1200 iterations. The square denotes the retina. Each intersection represents the centre of a receptive field and receptive fields of adjacent cells are connected by lines. (*b*) Typical receptive field. Connection strengths ($z$-axis) of one tectal cell to the retinal plane ($x$- and $y$-axes) are shown. The inlet shows a contour plot in which every contour corresponds to a step of 0.16.

factor, which depends on whether the model is one or two dimensional. The fibre–fibre interaction amplifies the growth of synaptic weights, if connections, which originate at nearby locations in the retina project to nearby locations in tectum. The range of these interactions is given by the widths of the Gaussian functions. In order to explain the results of the polarity reversal experiment, this interaction must act between fibres from different eyes and a sum over eyes has been added to equation (5).

We choose the Gaussian shape of interaction to incorporate the effect of locally adhesive markers (Bastmeyer *et al.* 1995). Thereby we assume rotational and translational symmetry. On the retina, the Gaussian function could represent similarity of chemical markers between one site and its neighbours. On the tectum, the Gaussian function could represent diffusion of chemical markers from the site of a retinal fibre or—if a small interaction width is chosen—the local interaction of surface bound markers. Note also, that on the retina, there is evidence for repulsive markers at mutually distant locations (Raper & Grunewald 1990). Distant repulsive markers can in principle be modelled by a Mexican-hat shaped (difference of Gaussians, DOG) retinal-interaction function. However, we may also regard the inhibitory component of such a function to be constituted by the retinal constraint of equation (8).

The expression

$$F^{\mathrm{act}}_{E\boldsymbol{\alpha}\boldsymbol{x}}(\boldsymbol{S}) = \sum_{\boldsymbol{\beta},\boldsymbol{y}} S_{E\boldsymbol{\beta}\boldsymbol{y}} g(|\boldsymbol{\beta}-\boldsymbol{\alpha}|,\sigma^{\mathrm{act}}_{\mathrm{ret}}) g(|\boldsymbol{y}-\boldsymbol{x}|,\sigma^{\mathrm{act}}_{\mathrm{tec}}) - \tfrac{1}{2} S_{E\boldsymbol{x}\boldsymbol{\alpha}}, \quad (7)$$

describes the activity-driven fibre–fibre interaction. It is similar to equation (5), except for the sum over eyes which is missing. Equation (7) is an instantiation of a correlation-based Hebbian learning rule (Linsker 1986*a*, *b*, *c*; Miller *et al.* 1989, 1994). The function $g(|\boldsymbol{\beta}-\boldsymbol{\alpha}|,\sigma^{\mathrm{act}}_{\mathrm{ret}})$ corresponds to the two-point correlation function of the afferent activity and is again taken to be Gaussian shaped and normalized. Its value denotes how often—on average—retinal cells at a distance $|\boldsymbol{\beta}-\boldsymbol{\alpha}|$ away from each other are activated synchronously. The function $g(|\boldsymbol{y}-\boldsymbol{x}|,\sigma^{\mathrm{act}}_{\mathrm{tec}})$ corresponds to the interaction function in the target area. It denotes the transfer of activity across tectum between cells which are separated by a distance $|\boldsymbol{y}-\boldsymbol{x}|$. Activity reaches the target cells is via the synaptic strengths $S_{E\boldsymbol{\beta}\boldsymbol{y}}$. Because no activity correlations are to be expected between both eyes, both eyes have to be treated separately and the sum over eyes had to be discarded.

Above mechanisms are complemented by a set of constraints which keep the connection weights bounded. The combination of $N$ with

$$C^{\mathrm{tec}}_{\boldsymbol{x}}(\boldsymbol{S}) = \eta_1 \sum_{D}^{\mathrm{eyes}} \sum_{\boldsymbol{\beta}}^{\mathrm{retina}} S_{D\boldsymbol{\beta}\boldsymbol{x}}$$

and

$$C^{\mathrm{ret}}_{E\boldsymbol{\alpha}}(\boldsymbol{S}) = \eta_2 \sum_{\boldsymbol{y}}^{\mathrm{tectum}} S_{E\boldsymbol{\alpha}\boldsymbol{y}}, \quad (8)$$

sets bounds on the total fan in and fan out of a tectal and a retinal cell, respectively. Together, these terms enforce a total connection strength which makes the expression

$$N - c^{\mathrm{tec}} C^{\mathrm{tec}}_{\boldsymbol{x}}(\boldsymbol{S}) - c^{\mathrm{ret}} C^{\mathrm{ret}}_{\boldsymbol{\alpha}}(\boldsymbol{S}), \quad (9)$$

close to zero. Evidence for a strong upper limit for the density of optic synapses on tectum was provided in the compression experiment of Murray *et al.* (1982), who found that the number of synaptic terminals per tectal area is similar to the undisturbed projection.

There is a (soft) upper limit for synapses also for a retinal fibre: less than half of the normal innervation density is formed when 20% of retinal fibres only are deflected to a tectum (Meyer 1994*b*). Although the constraint, (8), is formally symmetric with respect to retina and tectum, parameters can be chosen asymmetrically ($c^{\mathrm{tec}} > c^{\mathrm{ret}}$) to emphasize the tectal constraint.

### (*c*) *Computer implementation and model parameters*

Equation (1) is solved by the Euler method with a step size $\epsilon$, given in table 2. Negative weights are set to zero at every iteration, then a small amount of noise is added at every step (arbitrarily chosen equidistributed random numbers taken from the interval $[-0.000\,15, 0.000\,15]$). Initial conditions are given by small equidistributed random numbers from the interval $[0.002\,85, 0.003\,15]$ for all connection strengths. Convolutions are computed by fast Fourier transforms (Press 1988) with connection strengths set to zero close to the border of the retinal and tectal arrays, in order to implement open boundary conditions. Usually a grid of size $32 \times 32$ units was used for numerical simulations of the two-dimensional model with non-zero elements restricted to the inner $28 \times 28$ array. 64 units were used for the one-dimensional case, with non-zero elements restricted to the inner 56 units.

Table 2 summarizes the set of 'optimal' model parameters. Note that the following adjustments are made so that the model's behaviour is independent of the resolution: (i) the Gaussian interaction widths, $\sigma$, are given as a fraction of the number of units into one direction; (ii) the Gaussian functions (equation 6) are normalized to have the integral unity; and (iii) the $\eta$ scale inversely proportional to the resolution and are given different values for one- and two-dimensional simulations.

### (*d*) *Receptive fields and experimental procedures*

The centre $\boldsymbol{\beta}^*_{\boldsymbol{x}}$ of a receptive field of a tectal cell at site $\boldsymbol{x}$ is given by the expression

$$\boldsymbol{\beta}^*_{\boldsymbol{x}} = \frac{\sum\limits_{S_{\boldsymbol{\beta x}} > (1/2) S^{\max}_{\boldsymbol{x}}} S_{\boldsymbol{\beta x}} \cdot \boldsymbol{\beta}}{\sum\limits_{S_{\boldsymbol{\beta x}} > (1/2) S^{\max}_{\boldsymbol{x}}} S_{\boldsymbol{\beta x}}}, \tag{10}$$

in which $S^{\max}_{\boldsymbol{x}}$ denotes the numerically calculated maximal synaptic weight connected to neuron $\boldsymbol{x}$. The centre of the receptive field is calculated using connections with high weight only, in order to avoid boundary effects. The area of a receptive field of a tectal cell $\boldsymbol{x}$ is given by the number of (discrete) retinal sites $\boldsymbol{\beta}$ for which $S_{\boldsymbol{\beta x}}$ exceeds an arbitrarily chosen value of 0.003.

Table 3 finally summarizes the computer implementation of experimental procedures.

Table 2. *'Optimal' model parameters for the one-dimensional and the two-dimensional version of the model*

(Numbers in brackets denote parameter values for numerical simulations of two-eye experiments. The values of $\eta$ depend only on the dimension and on the resolution of the model.)

| model | linear one-dimensional | linear two-dimensional |
|---|---|---|
| interaction strengths | | |
| N | 1 | 0.3 |
| $a$ | 0.004 | |
| $f^{\mathrm{int}}$ | 0.5 | |
| $f^{\mathrm{act}}$ | 2 | |
| $c^{\mathrm{tec}}$ | 0.5 | 0.15 |
| $c^{\mathrm{ret}}$ | 0.5 | 0.15 |
| interaction ranges | | |
| $\sigma^{\mathrm{int}}_{\mathrm{ret}}$ | $\frac{3}{28}$ of retina | |
| $\sigma^{\mathrm{int}}_{\mathrm{tec}}$ | $\frac{1}{28}$ of tectum | |
| $\sigma^{\mathrm{act}}_{\mathrm{ret}}$ | $\frac{1}{28}$ of retina | |
| $\sigma^{\mathrm{act}}_{\mathrm{tec}}$ | $\frac{1}{28}$ of tectum | |
| compensation for size changes | | |
| $\eta_1$ | 0.5 | (1/2.4) |
| at size | 64 | $32 \times 32$ |
| $\eta_2$ | 0.5 | (1/2.4) |
| at size | 64 | $32 \times 32$ |
| numerically relevant parameters | | |
| $\epsilon$ | 0.05 (0.025) | 0.02 (0.01) |

## 4. RESULTS

In the following section the results of the numerical simulations are described. If not otherwise stated parameters were chosen according to table 2 for the standard grid size.

### (*a*) *Topographic maps*

Figure 3*a* shows the final topographic projection between retinal and tectal cells. The square represents retinal space, and each intersection of the grid corresponds to the centre $\boldsymbol{\beta}_{\mathrm{c}}(\boldsymbol{x})$ of a receptive field. Receptive field centres of cells $\boldsymbol{x}$ which are adjacent in tectum are connected by lines. From the fact that a regular lattice emerged, we conclude that a topographic projection is formed with a homogeneous magnification factor. Figure 3*b* displays the receptive field of a typical tectal cell. Receptive fields are of circular shape with maximum connectivity strength in the centre and continuously decreasing strengths away from it.

At the beginning of development, connections are randomly allocated and the fibre–tectum interac-

Table 3. *Numerical implementation of experimental procedures*

| experimental procedure | numerical implementation |
|---|---|
| removal of retinal or tectal graft | connections to this area are set to zero in every iteration |
| rearrangement of tectal graft | rearrangement of elements of the chemoadhesion matrix $A$ within the excised area |
| application of TTX | $f^{\mathrm{act}}$ is set to zero |
| deflecting fibres to ipsilateral eye | use of an additional retinal array |
| sectioning the optic nerve | reset synapse strengths to their initial random values |
| no sectioning of optic nerve | use result of normal map as initial condition |

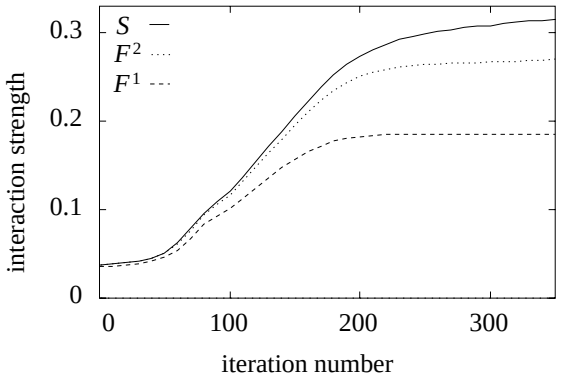


Figure 4. Synaptic strength and values of activity-dependent and intrinsic fibre–fibre interactions for one connection as a function of time for the one-dimensional model. The $x$-axis denotes iteration number, the $y$-axis shows from top to bottom the values of $S$, $f^{\mathrm{act}}$ and $f^{\mathrm{int}}$, without scaling by $f^{\mathrm{act}}$ or $f^{\mathrm{int}}$. The chosen weight connects the tectal cell to its receptive field centre.

tion is the only globally organized force. It ensures the correct polarity as well as rough topography, but remains constant. During refinement, fibre–fibre interactions increase because they scale with the connection strengths of neighbouring fibres (figure 4). Those interactions then ensure local topography as well as localized receptive fields.

Figures 5–7 show the simulation results obtained by the two-dimensional model. The topographic map is shown in figure 5*b*, the other experiments will be discussed in the following section.

### (*b*) *Specificity versus plasticity*

In all the following experiments fibre–fibre interactions favour a topographic map while fibre–tectum interactions try to enforce correct targeting and polarity. Both interactions compete during regeneration and—depending on the experimental paradigm—one or the other mechanism finally dominates.

In general, numerical implementations of the translocation and rotation experiments predict the experimental outcome only if the excised grafts are large enough and the fibre–tectum interaction is sufficiently strong. For small sized grafts, the fibre–fibre interactions of the surround override the influence of the fibre–tectum interaction within the translocated or rotated pieces and lead to a perfect topographic map. The influence of the relative strength of both interactions is explored in figure 8. The dashed line shows the number of 'successful' outcomes of the translocation experiments for the one dimensional case as a function of the parameter $a$ at a constant size of the excised tectal piece. For strong fibre–tectum interactions, model predictions are in accordance with the experiment.

While rotated and translated pieces of the projection are 'stable' for the one-dimensional model, this does not hold true in the two-dimensional case. As we can see in figure 5(*e*), as a result of a tectal graft translocation, the projection generally obeys a point–to–point projection at iteration 600. However, when the connections are strong and organized (figure 5*h*), until iteration 1800, fibre–fibre interactions override the fibre–tectum interaction in favour of larger topographically ordered patches. The reason is that tectal cells at the border between displaced and correct connections have double receptive fields (figure 9*a*). At these cells, the displaced and the orderly projecting retinal fibres compete and connections which have more neighbours of the same kind, hence stronger fibre–fibre interactions, will win. In one dimension, the number of neighbouring fibres from the original tectum always equals the number of neighbouring fibres from the graft, and 'reimplanted' grafts are stable. In the two-dimensional case the correctly projectioning neighbours outnumber the displaced fibres of small grafts and a topographic representation slowly replaces the disturbed projection. In the case shown, as observed by (Hope 1976), non-displaced tectal border areas are invaded by a displaced projection (figure 5*h*).

Figures 5*c*, *d* and 6*f* show the results of the expansion, compression and mismatch experiments. Model predictions match the experimental findings and the results are robust against parameter variations, i.e. any parameter may be varied by at least a factor of two.

When a part of the retina is removed without cutting the optic nerve, the remaining projec-

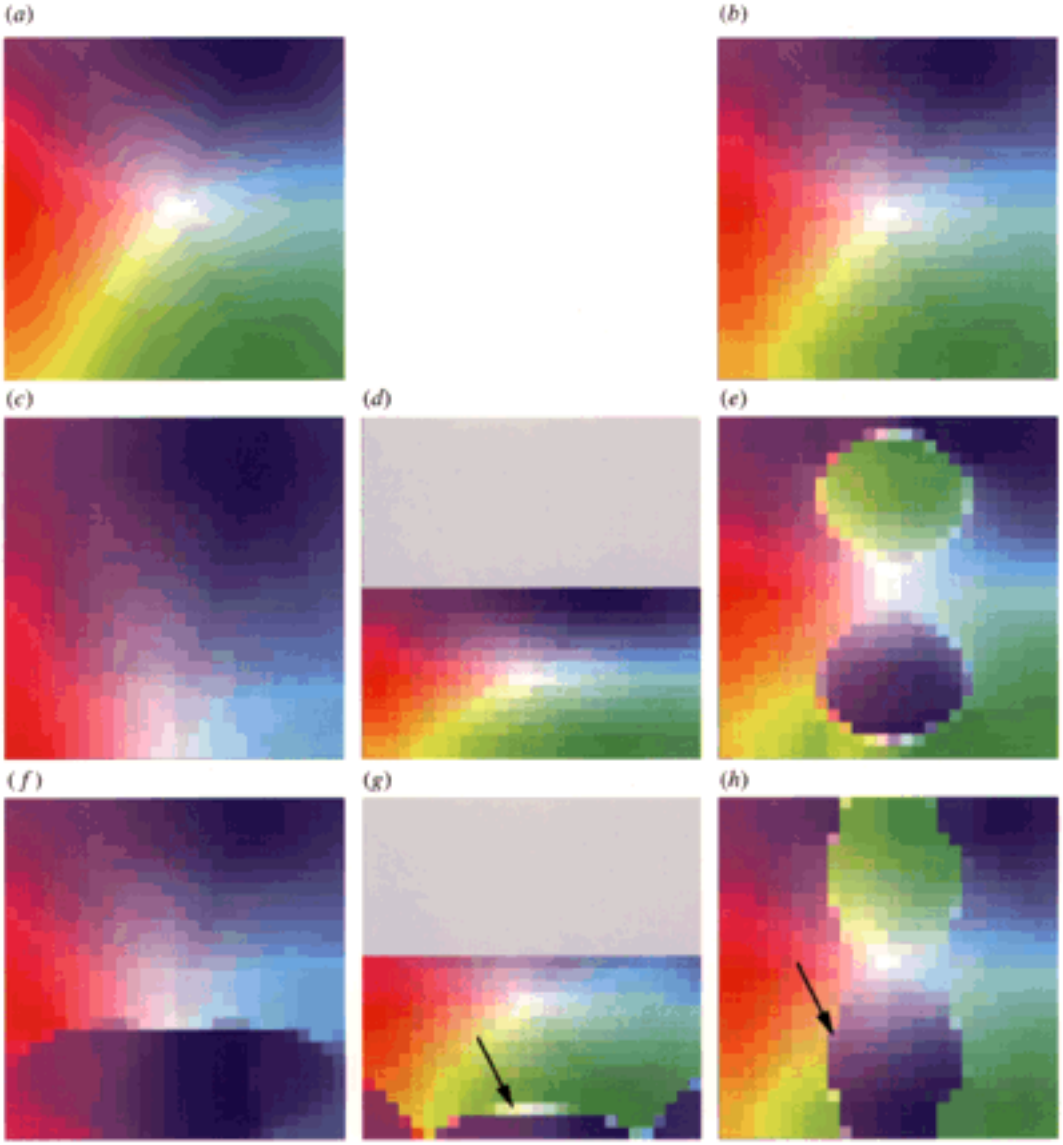


Figure 5. Simulation results for the two-dimensional model. (*a*) Shows the retinal array in which position is colour coded using a colour circle with decreasing hue towards the middle. Nasal is at the top, temporal at the bottom, ventral at the left and dorsal at the right. Pictures (*b*)–(*h*) show the tectal array in which posterior tectum is at the top, anterior at the bottom, medial to the left and lateral tectum to the right. The colour of every tectal cell (a small unicoloured square) denotes the centre of the receptive field, i.e. the retinal area from which the cell receives its main input (equation 10). For the following results, numbers in braces denote the numbers of iteration (the last iteration of a simulation is usually depicted). (*b*) *Normal topographic projection (1200)*. (*c*) *Expansion (1600)*: a nasal half retina was paired with a whole tectum. (*d*) *Compression (1300)*: an anterior half tectum receives fibres from an intact retina. (*e*) *Translocation (600)*: fibres grow into a tectum where an anterior graft has been exchanged with a posterior graft. (*f*) *True expansion (2600)*: as in (*c*), but as initial condition the (nasal) half retinal part of the normal projection at iteration 1200 maps to the posterior tectum. (*g*) *True compression (3000)*: as in (*d*), but as initial condition the (temporal) half retinal part of the normal projection at iteration 1200 maps to the anterior tectum. The other retinal fibres are allowed to invade the half tectum at iteration 1200. (*h*) *Translocation (1800)*: continuation of (*e*). Graft boundaries are not anymore obeyed by the projecting fibres. Arrows mark cells which receptive fields are shown in figure 9.

tion expands after several months (Schmidt 1978*a*) and remains topographic. When a part of the tectum is removed without cutting the optic nerve the projection compresses but topography is not fully restored (Gaze & Sharma 1970; Sharma 1972). Numerical simulations correctly predict the results of the compression experiment (figure 5*g*)—including the emergence of double receptive fields as one shown in figure 9*b*—but contradict the expansion results. Because the model is set up in a way that new connections are able to form everywhere across the denervated tectum, sprouting connections are not confined to the current border and topography is violated. This phenomenon is shown in figure 5*f* in

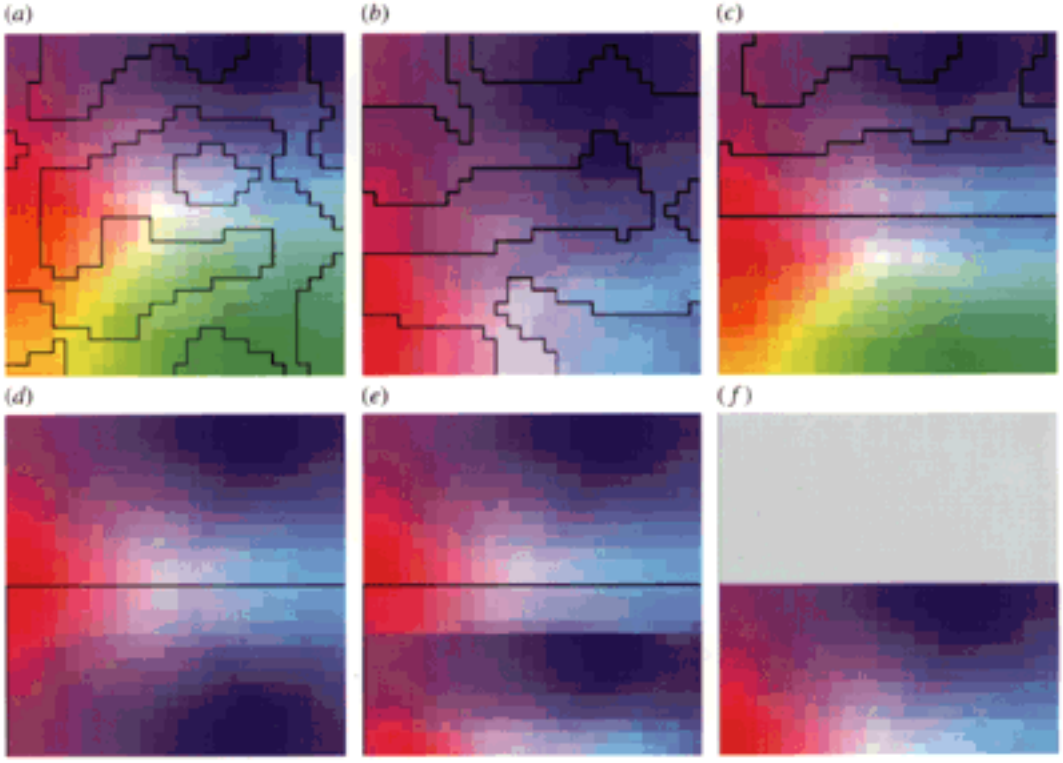


Figure 6. Simulation results for the two-dimensional model involving experiments with two eyes (*a*)–(*e*). Retinal positions of receptive field centres are colour coded as in figure 5. The border between areas of contralateral and ipsilateral eye-dominance is marked by a black line. Note that the learning rate, $\epsilon$, had to be halved for two-eye experiments. (*a*) *Two eyes (2400)*: two intact retinae project to the tectum. (*b*) *Double nasal expansion (2400)*: two nasal half retinae project to the tectum. (*c*) *One eye expansion (2500)*: a whole and a half retina project to the tectum. (*d*) *Meyer polarity reversal (3000)*: a nasal (ipsilateral) half retina is paired with a tectum. The initial condition is given by the normal projection between the contralateral, nasal half-retinal part and the posterior half of the tectum at iteration 1200. As a result the ipsilateral projection reverses its polarity along the anterior–posterior axis on the anterior half of the tectum. This is reflected by the colour changes along the axis from posterior to anterior tectum. (*e*) *Meyer polarity reversal (2200)*: for this experiment the fibre–tectum interaction is increased by setting $a = 0.006$. The fibre–tectum interaction now overrides the fibre–fibre interaction and the ipsilateral projection does not reverse. (*f*) *Mismatch (1300)*: one nasal half retina is paired with an (inappropriate) anterior half tectum. Fibres from central retina (white) 'shift' to the anterior border but polarity is preserved (cf. (*e*)).

which a topographic area only slightly larger than half of tectum is complemented by small locally topographic patches in the remaining area.

### (*c*) *The functional form of the fibre–tectum interaction*

So far, the double gradient function, equation (2) has been used to describe the form of the fibre–tectum interaction. As has been explained in model description, the double gradient function is characterized by intermediate specificity between retinal fibres and tectal locations. What happens, if interaction functions are used which: (i) are of similar specificity but of different functional form; (ii) are less specific, as in the case of the step-function (3); or (iii) enforce a much higher specificity, as in the case of the Lorentz-type function (4)? Numerical simulations performed for the one-dimensional version of the model provided the following results. Model predictions remain in accordance with experimental data if the double gradient function is replaced by single gradient, as has been suggested by Whitelaw & Cowan (1981). If a perfect step function is used, which is exactly zero in one half of tectum and retina and exactly one, polarity may not be correct for the expansion, compression or mismatch experiments. If the function, however, is slightly smoothed so that cues for correct polarity remain in each half, all experiments are explained. For the highly specific Lorentz-type function expansion, compression and mismatch are not predicted correctly. It is more favourable for the whole system if some axons are very much dislocated in favour of others to remain on their exact locations. In summary, the exact shape of the fibre–tectum interaction function does not really matter, as long as cues for the correct polarity are present and as long as the interaction is not too specific.

### (*d*) *Adhesion versus separation*

Other conflicting aims arise in experiments where the populations of both eyes meet. When an area


Figure 7. Eye-dominance maps for the simulation results of the two-eye experiments shown in figures 6*a–e*. Dark and light denotes contra and ipsilateral eye preference.

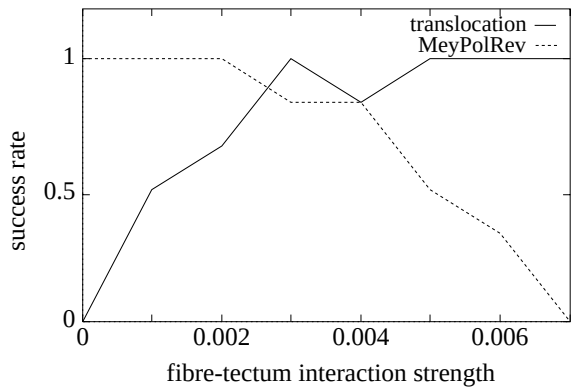


Figure 8. Polarity reversal versus tectal graft translocation. The percentage of successful experiments is plotted against the strength $a$ of the fibre–tectum interaction. Six simulations were performed per data point. We chose $a = 0.004$ as the 'optimal value'.

of tectum is doubly innervated the populations from the different eyes segregate locally into ocular dominance patches while global topography is preserved (figure 6*a*, two retinae and figure 6*b*, double nasal expansion). The segregation of fibres into patches of eye dominance occurs due to a conflict between the activity dependent fibre–fibre interactions, which encourages the formation of same-eye clusters, and the fibre–tectum interaction, which encourages the formation of topographic maps. This mechanisms become even more visible in experiments in which fibres from a whole retina and fibres from a nasal half retina jointly innervate one tectum (figure 6*c*).

The projection from the 'spare' nasal half of the retina stays confined to the appropriate part of tectum but forms ocular dominance patches with the rivalling part of the other projection. This is very much in accordance with the observations by Schmidt (1978*a*).

Figure 6*d* shows model predictions of the polarity reversal experiment of Meyer (1979*a*). This experiment enforces a conflict between the fibre–tectum and the intrinsic fibre–fibre interaction. As in the corresponding experiments, the intrinsic fibre–fibre interaction dominates and leads to a reversal of polarity of the map which is newly formed in the rostral part of the tectum. An analysis of the regeneration dynamics shows two phenomena which are critical to the outcome of the experiment, as follows. (i) The contralateral projection occupies relevant parts of the anterior tectum, if this part is not soon innervated by ipsilateral fibres. Then patches of contralateral and of the deflected projection are not confined to one half of the tectum only (compare double nasal expansion). (ii) The intrinsic fibre–fibre interaction between fibres from the centre of the contralateral retina and the ingrowing fibres from the ipsilateral retina must be large enough to override the competing fibre–tectum interaction.

At this point simulation results are brittle: when the strength of the fibre–tectum interaction is increased by 50% ($a = 0.006$), polarity remains

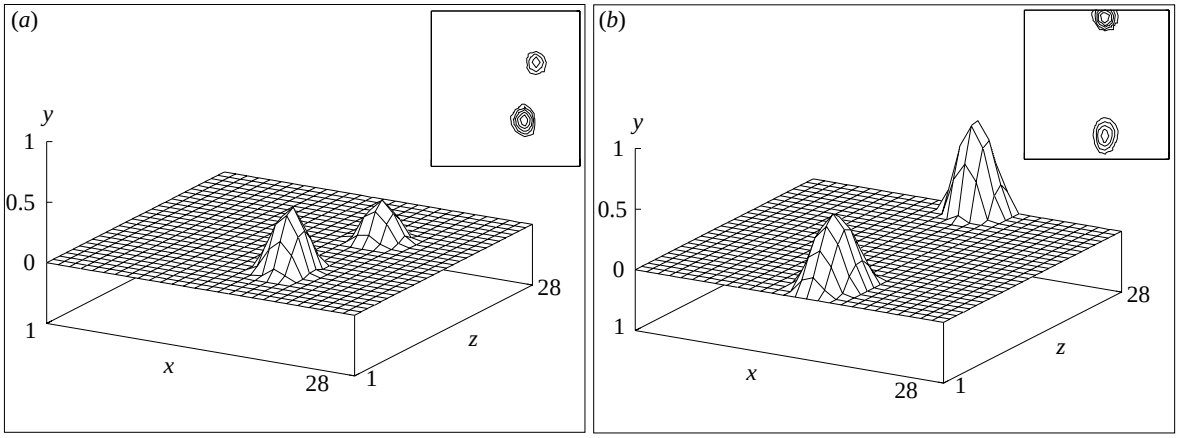


Figure 9. Bi-lobed receptive fields (*a*) in the translocation experiment shown in figure 5*h* and (*b*) in the 'true compression' experiment shown in figure 5*g*. Representation as in figure 3*b* with contours in the inlets corresponding to steps of 0.09 (*a*) and 0.12 (*b*).

unreversed in nearly the whole anterior tectum (figure 6*e*). If, for example, the strength of the interfibre interaction is set to zero the polarity remains unreversed similar to the mismatch experiment.

More than any other experiment the polarity reversal experiment contradicts specificity. The solid line in figure 8 shows the percentage of polarity reversals as a function of the strength, $a$, of the fibre–tectum interaction. Polarity does not reverse if $a$ is increased by more than 50% over the current parameter setting. In the parameter regime around the current settings we observe that most of the posterior ipsilateral projection does reverse. A small part along the anterior border retains its proper polarity, similar to what is sometimes observed in the experiments of Meyer (1979*a*). For low values of $a$ reversal becomes the dominant phenomenon.

Note, however, that when $a$ becomes too low, the translocation experiment does not show the correct outcome. Hence there exists only a small parameter window, where the outcome of all competing experimental scenarios is predicted correctly.

### (*e*) *The role of activity*

When the activity-dependent fibre–fibre interaction is set to zero, the model predicts the following phenomena: (i) segregation into eye-dominance patches does not occur; (ii) the size of receptive and projective fields remains large (see next section). Note that the segregation of fibres occurs also if the activity-dependent interaction is set to zero only within one eye. In this case cells selective for the activity-blocked retina are confined to the edges of tectum (data not shown). This is obviously a minimum in the model's energy function, because the active fibres exert a stronger mutual interaction away from the border. Otherwise, predictions remain unchanged, i.e. the qualitative outcome of all other experiments does not depend on the activity-dependent fibre–fibre interaction, for the set of parameters given in table 2.

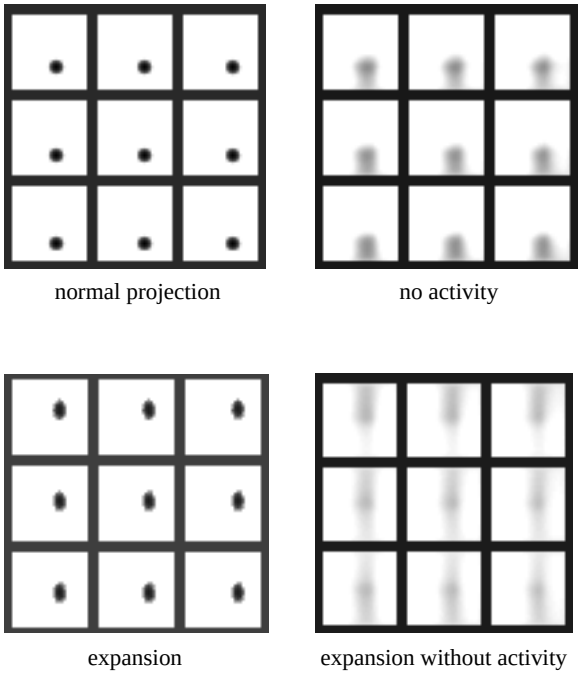


Figure 10. Simulation results of projective fields for normal development, expansion, normal development under block of activity and expansion under block of activity. Each figure shows the projective fields of nine neighbouring retinal cells. Each square denotes the whole tectum, posterior at top, anterior at bottom. Connection strengths to the corresponding tectal cells are coded by grey values. The pictures of the normal projection and the expansion experiment were taken at iteration 1200, when the map was mature. The pictures on the right where no activity is present are taken at iteration 2800. At this time, also the activity-blocked projection nearly converged (see figure 11).

### (*f*) *The size of receptive and projective fields*

Figure 10 shows final projective fields. The projective fields under block of activity are diffuse, weak and large in comparison to the fields which emerge when activity is present. Projective fields under the

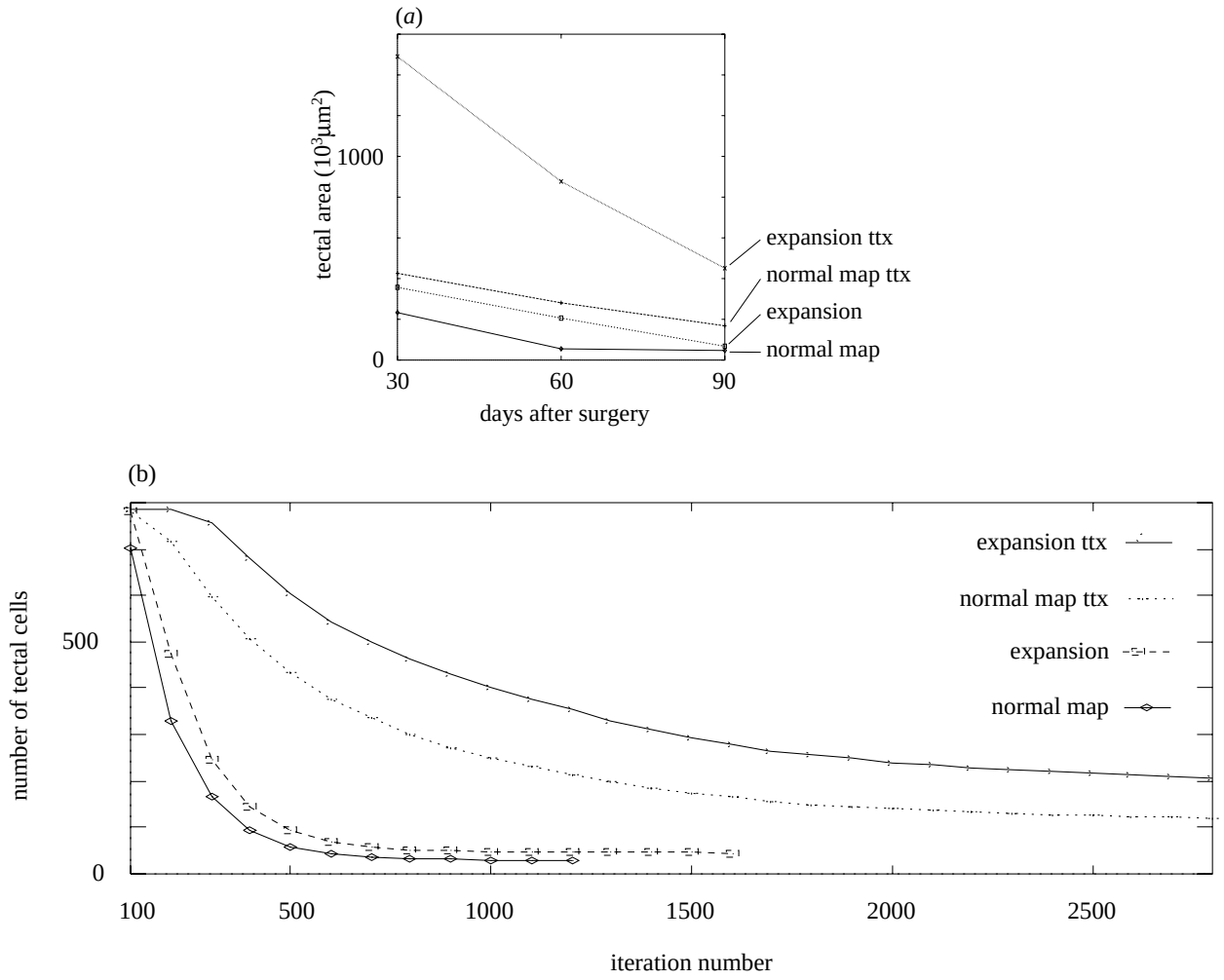


Figure 11. Size of projective fields as a function of time during regeneration for the experimental paradigms described in figure 10. (*a*) Experimental data taken from Olson & Meyer (1994). (*b*) Results of numerical simulations. The projective field size (number of tectal cells) is averaged over retinal cells.

expansion paradigm are elongated along the rostrocaudal axis. Figure 11 shows the development of the size of receptive and projective fields for four different experimental paradigms: normal regeneration, regeneration under activity blockade with TTX, expansion and expansion under TTX. Model predictions are compared with experimental data obtained by Olson & Meyer (1994). Projective fields shrink slowest and/or remain largest for expansion under TTX followed by normal development under TTX, expansion and normal development, similar to what is observed experimentally. For normal development under TTX, however, the model predicts broader receptive fields than one would have expected from the experimental data.

### (*g*) *The influence of the range of interactions*

Figure 12 shows the percentage of successful translocation experiments as a function of the widths of the intrinsic fibre–fibre interaction within retina, $\sigma_{\mathrm{ret}}^{\mathrm{int}}$, and tectum, $\sigma_{\mathrm{tec}}^{\mathrm{int}}$. Primarily, translocation is observed with a small $\sigma_{\mathrm{tec}}^{\mathrm{int}}$ only, and the experiment fails when $\sigma_{\mathrm{tec}}^{\mathrm{int}}$ is large and $\sigma_{\mathrm{ret}}^{\mathrm{int}}$ is small at the same time. How can this finding be explained? The translocation (as well as the rotation) experiments break the symmetry of the fibre–tectum interaction function with respect to the interchange of retinal and tectal coordinates in equation (2). A small tectal interaction width $\sigma_{\mathrm{tec}}^{\mathrm{int}}$ favours a positive outcome of the translocation experiment because a long-range interaction across the borders between translocated and intact tissue would not allow populations from differing parts in the retina to remain adjacent. A large retinal interaction width $\sigma_{\mathrm{ret}}^{\mathrm{int}}$ favours a positive outcome because—due to normalization of the Gaussian functions—the proportion of effective connections which are adjacent in retina and in tectum decreases.

When $\sigma_{\mathrm{ret}}^{\mathrm{int}}$ is decreased to the size of $\sigma_{\mathrm{ret}}^{\mathrm{act}}$ which is one, then this prevents also the emergence of specificity for one eye. Figure 13 shows that in this case all cells remain binocular. Again the reason is that with a small interaction width the interfibre interaction couples effectively strong connections from different eyes within a small region and prevents the uncoupled development of eye-specific clusters.

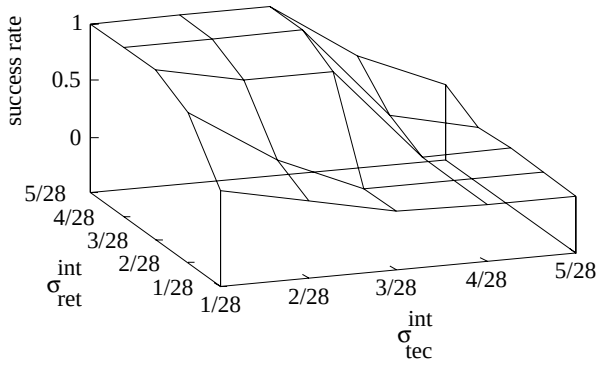


Figure 12. Percentage of successful translocation experiments for the one-dimensional model as a function of the widths of the intrinsic fibre–fibre interaction. Axis to the right: interaction width $\sigma_{\mathrm{tec}}^{\mathrm{int}}$ within tectum; axis to the left: interaction width $\sigma_{\mathrm{ret}}^{\mathrm{int}}$ within the retina. The vertical axis shows how often out of six simulations the results match the biological example in that a displaced projection occurs to the exchanged grafts.

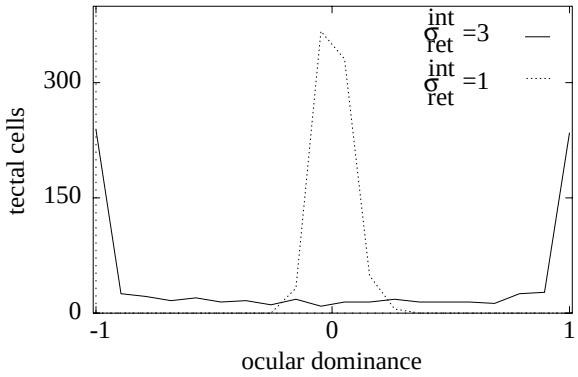


Figure 13. Number of cells as a function of eye dominance for different widths of the retinal interaction function ($\sigma_{\mathrm{ret}}^{\mathrm{int}} = 3$, normal setting, curve with peaks at $-1$ and 1 or $\sigma_{\mathrm{ret}}^{\mathrm{int}} = 1$, curve with a peak at 0). The other parameters remain unchanged. The ocular dominance value for a tectal cell $x$ is calculated by $(2\sum_{\alpha} S_{1\alpha x}/\sum_{D}\sum_{\alpha} S_{D\alpha x}) - 1$. Values of 1 and $-1$ denote dominance for the eyes. This range is divided into 40 bins and the number of cells of the corresponding specificities for the two-dimensional setup are plotted.

## 5. DISCUSSION

The results of the previous section have shown that three mechanisms and a set of constraints are sufficient to explain a large body of experimental data about the formation of the retinotectal projection in goldfish. In the following we will first discuss the three mechanisms separately, then comment on their interaction and finally discuss model assumptions and model predictions in the biological context.

### (*a*) *Intrinsic fiber–tectum interactions*

Intrinsic fibre–tectum interactions may in principle fulfil different functions: (i) they allow afferent fibres to distinguish between tectal and non-tectal tissue; (ii) they enable afferent fibres to find a specific neuronal layer in tectum; (iii) they establish the correct polarity of the topographic projection; and (iv) they guide fibres to their exact location in tectum. The first two functions are not within the scope of our model. The last point is supported mainly by the tectal graft translocation experiment, while all other experiments indicate their predominant role in establishing the correct polarity. TTX experiments, for example, impose limits on the precision of the fibre–tectum interaction, because wiring precision is reduced when there is no activity dependent refinement present.

More evidence is provided by our numerical simulations which show that the fibre–tectum interaction must not be too specific. A highly specific fibre–tectum interaction like the Lorentz-type function, (4), would not allow aberrations of axons from their appropriate target positions, hence contradicting the compression, expansion and mismatch experiments.

This kind of function punishes small deviations from the appropriate target area nearly as much as large deviations. Thus, in an expansion experiment, the more fibres project exactly to their correct positions, the more favourable for the whole system. This causes remaining fibres to make distant misprojections to otherwise unoccupied tectal areas. In many expansion experiments no such behaviour has been observed. Consequently a convex function seems to be appropriate, which slowly loses influence near the correct position but strongly at a distance.

Tectal-graft translocation may occur for 'soft' fibre–tectum interactions, as our simulations show, but results are somewhat brittle. This is in accordance with experiments. In addition, one has to keep in mind that the translocation experiments may not have been 'clean' enough to exclude effects of the previous tectal innervation. 'Clean' experiments have—so far—only been performed for tectal graft rotation in *Xenopus* (Hunt 1976; Straznicky 1978). Even with a step function as in equation (3), the results did not differ significantly from the results using the 'double-gradient' form. To preserve polarity in an experiment with only one half retina or tectum, however, the steps have to be smoothed. Thus, model predictions are not brittle with respect to the particular form chosen, especially when specificity is reduced.

Experimental evidence is strong for graded distributions of markers because these have been discovered recently in retino-tectal systems (Drescher *et al.* 1995; Cheng *et al.* 1995), but somewhat softened stepfunctions of chemical gradients in retina (McLoon 1991) and additionally in tectum are also plausible. Recent findings suggest that a molecule(s) expressed by engrailed genes attracts nasal retinal axons and at the same time repels the growth of temporal axons (Friedman & O'Leary 1996; Itasaki & Nakamura 1996). The issue is not decided, and mapping along the medio-lateral axis remains unclear, hence variability of fibre–tectum interactions is still 'allowed' and should be explored in mathematical analyses.

### (*b*) *Intrinsic fibre–fibre interactions*

Several experimental observations, *in vivo* and *in vitro*, justify the existence of a fibre–fibre interaction independent of activity.

(1) The polarity reversal experiment requires a fibre–fibre interaction between eyes (thus independent of correlated activity) which overrides the basic polarity information provided by fibre–tectum interactions.

(2) Temporal retinal fibres remain confined to the corresponding rostral half tectum, if the tectum already hosts a normal map of the other eye (Schmidt 1978*a*).

(3) Even when activity is blocked, the projection of a half retina expands topographically across the whole tectum, if the second half is surgically removed. At least for some possible forms of fibre–tectum interactions and growth constraints this result suggests that an activity-independent fibre–fibre interaction supports such a homogeneous projection. The enlarged receptive and projective fields measured in the experiments of Meyer (1994*b*) suggest larger interaction widths of this function compared to the activity-driven interaction.

(4) In an *in vitro* assay (Raper & Grunewald 1990) nasal retinal fibres repel temporal (and thus distant) retinal fibres. Here temporal growth cones collapse on contact with nasal fibres when they meet at a Y-shaped junction.

(5) The expression of some cell adhesion molecules is growth associated. The E587 cell surface glycoprotein is expressed on young retinal axons (Bastmeyer *et al.* 1995). In the fish retina these originate from the ciliary margin where cells proliferate. Hereby fibres adhere together and fasciculate in an age-related (and to a certain limit topographic) order.

(6) Guidance molecules, e.g. netrins in rat and chick, have been found which show repellent or attractive activities on different types of fibres (see Holt & Harris 1993, for a review).

The first three experiments provide evidence for fibre–fibre interactions active after the afferents reach tectum, though in an indirect fashion. The first experiment requires this interaction for the reversal of map polarity. If the intrinsic fibre–fibre interaction parameter $f^{\mathrm{int}}$ is set to zero we observe in the second experiment an expansion of the half-retinal fibres across the whole tectum and in the third experiment receptive and projective fields do not condense. Note, that increasing the fibre–tectum parameter, $a$, by a factor of more than 50 confines half-retinal fibres to the appropriate half and condenses projective and receptive field sizes properly (one-dimensional simulation). However, the polarity reversal, then is impossible. The latter three experiments provide direct evidence for fibre–fibre interactions via molecular markers, though at an earlier stage (in the optic pathway). Their influence on the tectum is not clearly characterized. To abstract from inhomogeneity of marker distributions we describe the intrinsic neighbour–to–neighbour interaction uniformly by Gaussians. It is plausible to assume the expression of the markers to be proportional to fibre material and to scale the interaction proportional to synaptic strengths. The interaction widths could not be chosen large in the tectum (figure 12), but they were in the retina, to match experimental results.

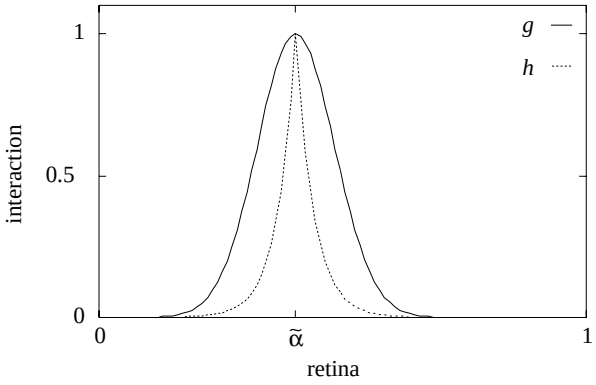


Figure 14. Interaction functions, $g$, of this model and $h$, of the model by Cowan & Friedman which are due to intrinsic markers. The $x$-axis denotes the retina which is scaled as in equation (2). Functions are centred at an arbitrary cell location $\tilde{\alpha}$.

Interaction widths do not scale with the size of the projective and receptive fields, because they only depend on retinal (intrinsic marker distribution) and retinal-fibre properties (fibre-bound markers and/or diffusion of retinal markers from the site of a retinal fibre), which we assume to be constant during regeneration. The small interaction width chosen for the tectum suggests fibre-bound markers, but does not exclude diffusion of those markers within a short range.

Cowan & Friedman (1991) show that graded marker distributions can account for highly specific interactions also in the retina. They assume two gradients in the retina where one is distributed like $\tilde{\alpha}$, the other like $1-\tilde{\alpha}$, where $\tilde{\alpha}$ represents a scaled retinal cell location as in equation (2). They further assume these markers to be self-adhesive (homophilic) such that each molecule binds to a replica of itself on another fibre at $\tilde{\beta}$, with excess molecules not binding at all. The interaction between markers which are involved in binding results in an effective fibre–fibre interaction of the form

$$\min(\tilde{\alpha},\tilde{\beta}) + \min(1-\tilde{\alpha}, 1-\tilde{\beta}) = 1 - |\tilde{\alpha}-\tilde{\beta}|. \qquad (11)$$

This function decreases linearly away from its maximum at $\tilde{\alpha}=\tilde{\beta}$. Higher specificity is achieved if the binding force is of exponential form

$$\begin{aligned} h(\boldsymbol{\alpha}-\boldsymbol{\beta}) &= \exp[\gamma_1(1-|\tilde{\alpha}-\tilde{\beta}|)] \\ &= \gamma_2 \exp[-\gamma_1|\tilde{\alpha}-\tilde{\beta}|], \end{aligned} \qquad (12)$$

with $\gamma_1$ and $\gamma_2$ being arbitrary constants. Figure 14 compares function (12) with the retinal interaction function used for the intrinsic fibre–fibre interaction in equation (5).

The model of Cowan & Friedman (1991) also introduces a 'history trace' of fibre-bound markers in order to simulate the debris of retinal fibres which

temporarily remains on the tectum for some of the reported regeneration experiments. When an explicit debris term is included the model can account for experimental results obtained for example by Yoon (1975*a*) and Schmidt *et al.* (1978*b*) who showed that immediately after the cut of the optic nerve ingrowing fibres are attracted to those tectal sites which have previously been innervated by fibres from the same retinal location. As a result a projection pattern which mirrors the previous innervation may intercalate with a map which would arise in 'clean' regeneration experiments. The influence of debris decreases in time.

The influence of debris has not been included in the model discussed in this paper, hence equation (1) cannot account for the corresponding experiments. Note, however, that debris may not be regarded as an actual 'developmental process' so there is no need to add it to the current framework. The current model, however, can be extended to account for debris, along the lines suggested by the work of Cowan & Friedman (1991).

### (*c*) *The activity dependent fibre–fibre interaction*

There is ample evidence for activity-dependent processes from pharmacological blocks by, e.g. TTX, AP5 or AP7.

(1) The two-eye experiments show that activity is responsible for the segregation of the two populations into ocular dominance patches.

(2) One-eye experiments demonstrate the role of activity-dependent sharpening of the projection. The width of this interaction has been estimated through the sizes of projective and receptive fields in the undisturbed topographic projection.

The activity-driven fibre–fibre interaction mediates growth enhancement of neighbouring fibres but only if they originate from the same retina. The segregation between left-eye and right-eye populations is a result of this selective clustering given the constraint that a tectal cell has at the same time an upper bound of innervation. The stripe like pattern of ocular dominance bands, however, is due both to the topographic representation of the retinal maps or, if the fibre–tectum interaction is set to zero, to a nearby representation of corresponding retinal sites of different eyes through the intrinsic fibre–fibre interaction.

The sharpening effect of this mechanism is due to the smaller interaction width $\sigma_{\mathrm{ret}}^{\mathrm{act}}$ compared to the intrinsic fibre–fibre interaction. The interaction widths $\sigma_{\mathrm{ret}}^{\mathrm{int,act}}$ and $\sigma_{\mathrm{tec}}^{\mathrm{int,act}}$ are of different origin. While the width of an activity-dependent interaction of the Hebbian kind depends on the two-point correlation function (Linsker 1986*a*, *b*, *c*; Miller *et al.* 1989) of the afferent activity patterns in the retina and on the range of lateral interactions in tectum, the range of the intrinsic interaction is most likely determined by chemical markers. Consequently, one would expect different interaction ranges.

In our model, the interaction kernels for the activity-dependent interactions are modelled via Gaussian kernels, which incorporate the assumptions of local correlations in the activity patterns and local lateral interactions in tectum. If one combines the activity driven fibre–fibre interaction with the constraints of equation (8), however, a net interaction results which is locally excitatory but globally inhibitory. This interaction is similar to the DOG interactions which are typically assumed by correlation based models (Linsker 1986*c*; Miller *et al.* 1989; Miller 1994; Piepenbrock *et al.* 1996; Stetter *et al.* 1994). There is, however, a formal difference between our ansatz and typical correlation based learning models. In correlation-based learning, the fibre–tectum interaction acts multiplicatively via the 'arbor function' and modulates the strength of the activity driven fibre–fibre term, while in our model fibre–tectum and fibre–fibre interactions are additively combined. The differences between both approaches will be discussed elsewhere.

### (*d*) *Constraints*

The precise form of constraints cannot be directly deduced from experimental findings, however, their presence is necessary for the model to correctly predict the data. Synaptic weights in a linear model without constraints would diverge to infinite strength. Synaptic strengths are kept finite by a subtractive constraint, equation (8), for the total fan in and fan out, a decay term in equations (5) and (7), and a hard lower bound of synaptic weights at zero. Constraints are motivated by the fact that the afferent retinotectal fibres are all excitatory, and by experimental evidence that the number of tectal target sites is conserved (Murray *et al.* 1982; Hayes & Meyer 1988). A study by Prestige & Willshaw (1975) showed that the outcome of mismatch and expansion experiments cannot be explained if no kind of competition is enforced by constraints. If we test our one-dimensional model without retinal constraint ($c^{\mathrm{ret}} = 0$), then the whole tectum will be innervated by retinal cells from a small region the size of a receptive field only. Analogously, without a tectal constraint ($c^{\mathrm{tec}} = 0$) all incoming fibres will concentrate on a small cluster of tectal cells.

In principle there are several ways of restraining synaptic weights, like hard bounds and the multiplicative constraints often used in models of Hebbian learning (Piepenbrock *et al.* 1997), or additional nonlinear decay terms added to equation (1). Our objective was to keep constraints simple, yet biologically interpretable. A detailed study of the influence of constraints is currently being performed.

### (*e*) *Multiple forces*

Following Occam's razor it is desirable to explain the development of patterns in the brain with a minimum number of mechanisms. Taking into account the current experimental evidence we arrive at three growth mechanisms restrained by three constraints. This selection of mechanisms is similar to the model of Fraser & Perkel (1990), except that there, the intrinsic interaction between fibres of different eyes

Table 4. *The two columns to the left show the growth mechanisms of two models, the multiple constraint model (MCM; Fraser 1990) and this model (lin)*

(The columns to the right show the parameters by which these mechanisms contribute to growth in the two models.)

| MCM | lin | MCM | lin |
|---|---|---|---|
| mechanisms | | parameters | |
| $G_{\mathrm{C}}$ | $N$ | 1000 | 0.300 |
| $G_{\mathrm{FT}}$ | $A$ | 25 | 0.004 |
| — | $F^{\mathrm{int}}$ | — | 0.500 |
| $G_{\mathrm{FF}}$ | $F^{\mathrm{act}}$ | 0.025 | 2.000 |
| $G_{\mathrm{RN}}$ | $C^{\mathrm{tec}}$ | −2 | −0.150 |
| — | $C^{\mathrm{ret}}$ | — | −0.150 |

and a retinal constraint term similar to $C^{\mathrm{ret}}$ are lacking. Because a unit of the *multiple constraint model* is a whole retinal arbor, rather than some synaptic efficacy, uncontrolled growth of a retinal cell's arbor on the tectum cannot emerge. Therefore, there is no need for a retinal constraint term like $C^{\mathrm{ret}}$ or a synaptic decay. The omission of the intrinsic fibre–fibre term, however, makes the model less powerful in interpreting the data.

Table 4 directly compares both models with respect to the weights they give to the different mechanisms. From table 4 it becomes apparent that the fibre–tectum interaction in the *multiple constraint model* is effectively stronger than the fibre–fibre term (for proper comparison, $G_{\mathrm{FT}}$ has to be multiplied by the percentage of tectal area which is occupied by a retinal arbor, this is 1%). This is due to the fact, that the *multiple constraint model* does not try to predict the polarity reversal experiments: in order to correctly predict polarity reversal, the fibre–tectum interaction function had to be decreased way beyond the fibre–fibre term. Thus we arrived at a parameter regime which is close to the lower bound to the fibre–tectum interaction strength set by the translocation experiment and rotation experiments.

In our model the fibre–tectum interaction is the inhomogeneity in a linear equation and does not scale with the strength of synaptic weights as the other mechanisms do. It is relatively strong in the beginning of the simulation when the projection is weak, but it loses influence as soon as connections grow. This shift from one mechanism being dominant to another occurs without change of parameters but only through the dynamics of the observed variables which are the synaptic efficacies.

### (*f*) *Summary*

We have shown that the regeneration of the retinotectal projection in goldfish can be described by a simple, almost linear, developmental model which is based on three kinds of mechanisms with biologically plausible constraints. The model explains all relevant experiments with the same set of parameters, including experiments on the size of receptive and projective fields, and illustrates well the cooperation and competition of the different mechanisms for the different experimental paradigms. In particular, the model illustrates how the differing mechanisms interact and shows that no experiment performed so far has been able to single out one of the mechanisms involved, except for the blockade of electrical activity.

Given the universality of mechanisms in neural development we expect that our modelling framework will not only shed light on the development of the retinotectal projection in goldfish but will be applicable to the formation of the topographic projections between layers of cells in general. Candidates are the formation of the projection in other lower vertebrates, e.g. the zebrafish system in which mutagenesis experiments recently lead to a wealth of data (Nüsslein-Volhard 1994), and the development of projections in the visual pathways of mammals, in which fibres from more than two populations of cells converge and in which evidence for the importance of intrinsic processes is growing. These issues are subject of further investigations.

We thank Professor K. Schulten and the Resource of Concurrent Biological Computing (University of Illinois, Urbana) for hardware and software support. Computing time on the CM5 was made available by HLRZ Jülich and NCSA (Urbana, USA). The project was funded in part by HFSPO (RG 98/94B), DFG (Ob 10212-1) and by a NATO collaborative grant (CRG 950694).

## APPENDIX 1. ANALYSIS OF THE MODEL: AN ENERGY FUNCTION

Let $\boldsymbol{S}$ be the $R \cdot T$-dimensional vector that describes the value of all connection strengths at a given time, i.e. the state of the whole projection. Its derivative $\dot{\boldsymbol{S}}$ is given by equation (1). Without the constraint that connection strengths are all positive $\dot{\boldsymbol{S}}$ satisfies the condition

$$\frac{\partial \dot{S}_\mu}{\partial S_\nu} = \frac{\partial \dot{S}_\nu}{\partial S_\mu}, \quad \forall\ \mu, \nu \text{ among } \boldsymbol{\alpha} \text{ or } \boldsymbol{x}. \tag{13}$$

and equation (1) implements a gradient descent procedure minimizing the cost function, $U$,

$$\begin{aligned} U(\boldsymbol{S}) = -\sum_{E}^{\text{eyes}} \sum_{\boldsymbol{\alpha}}^{\text{retina}} \sum_{\boldsymbol{x}}^{\text{tectum}} S_{E\boldsymbol{\alpha},\boldsymbol{x}} (N + aA_{\boldsymbol{\alpha},\boldsymbol{x}} \\ + f^{\mathrm{int}} F^{\mathrm{int}}_{\boldsymbol{\alpha x}}(\boldsymbol{S}) + f^{\mathrm{act}} F^{\mathrm{act}}_{E\boldsymbol{\alpha x}}(\boldsymbol{S}) \\ - c^{\mathrm{tec}} C^{\mathrm{tec}}_{\boldsymbol{x}}(\boldsymbol{S}) - c^{\mathrm{ret}} C^{\mathrm{ret}}_{E\boldsymbol{\alpha}}(\boldsymbol{S})), \end{aligned} \tag{14}$$

i.e.

$$\dot{\boldsymbol{S}} = -\nabla_{\boldsymbol{S}} U(\boldsymbol{S}). \tag{15}$$

The cost function, $U$, is of second order in $\boldsymbol{S}$. Consequently, there exists exactly one fixed point which

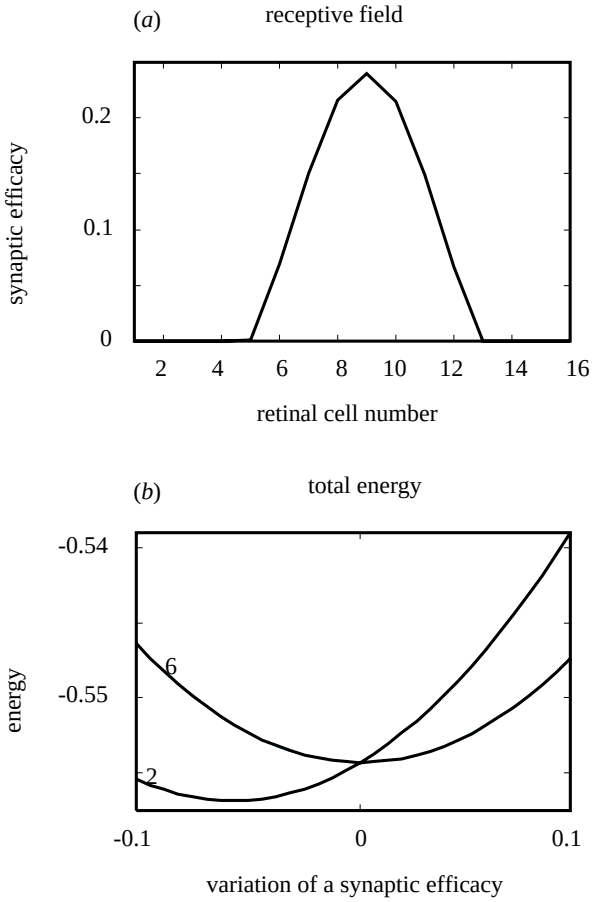


Figure 15. (*a*) Stationary synaptic weights ($y$-axis) for one tectal neuron which is connected to a retina of 16 cells ($x$-axis). (*b*) Cost, $U$, ($y$-axis) as a function of the difference of the synaptic efficacy to its stationary value ($x$-axis). Efficacies to retinal cells two and six were varied individually while keeping others constant. Parameters were $N = 1$, $a = 0$, $f^{\mathrm{int}} = 0$, $f^{\mathrm{act}} = 2$, $\sigma^{\mathrm{act}}_{\mathrm{ret}} = \frac{8}{3}$, $c^{\mathrm{tec}} = 1$, $c^{\mathrm{ret}} = 0$.

can be either a minimum, a maximum or a saddle point.

The stationary state is given by

$$\dot{\boldsymbol{S}} = A \cdot \boldsymbol{S} + \boldsymbol{b} = 0, \tag{16}$$

where the product $A \cdot \boldsymbol{S}$ is a shorthand notation for the mechanisms $F^{\mathrm{int}}_{\boldsymbol{\alpha x}}(\boldsymbol{S})$, $F^{\mathrm{act}}_{E\boldsymbol{\alpha x}}(\boldsymbol{S})$, $C^{\mathrm{tec}}_{\boldsymbol{x}}(\boldsymbol{S})$ and $C^{\mathrm{ret}}_{E\boldsymbol{\alpha}}(\boldsymbol{S})$, which are linear in $\boldsymbol{S}$, and the vector $\boldsymbol{b}$ includes the expressions $N$ and $A_{\boldsymbol{\alpha},\boldsymbol{x}}$, which are constant in $\boldsymbol{S}$.

For a simplified system consisting of one tectal cell and a single one-dimensional retina equation (16) was solved by a Gauss–Jordan algorithm (Press 1988). Let $\sigma$ be the width of the fibre–fibre interactions within the retina. For very large retinal $\sigma$ the stationary state is characterized by $\boldsymbol{S}$ being positive across the whole retina, and the fixed point corresponds to a minimum of the cost function, $U$.

For biologically realistic values of $\sigma$ the matrix, $A$, of equation (16) has positive and negative eigenvalues and the fixed point corresponds to a saddle point and is thus unstable. Consequently, all stationary solutions of equation (1) correspond to border minima, which generated by the requirement of all synaptic weights to be positive.

Figure 15*a* shows the stationary connection strengths for one tectal neuron which makes connections to a retina consisting of sixteen cells. Some of the weights become zero which indicates that the stationary state corresponds to a border minimum. Figure 15*b* shows a plot of the cost, $U$, as a function of the difference between connection strengths and their stationary values. As expected, the energy, $U$, is minimal only for those weights which do not vanish.

## REFERENCES

Baier, H. & Bonhoeffer, F. 1992 Axon guidance by gradients of a target-derived component. *Science* **255**, 472–475.

Bastmeyer, M., Ott, H., Leppert, C. & Stuermer, C. 1995 Fish E587 glycoprotein, a member of the l1 family of cell adhesion molecules, participates in axonal fasciculation and the age-related order of ganglion cell axons in the goldfish retina. *J. Cell Biol.* **130**, 969–976.

Cheng, H., Nakamoto, M., Bergemann, A. & Flanagan, J. 1995 Complementary gradients in expression and binding of elf-1 and mek4 in development of the toppographic retinotectal projection map. *Cell* **82**, 371–381.

Cook, J. & Rankin, E. 1986 Impaired refinement of the regenerated retinotectal projection of the goldfish in stroboscopic light: a quantitative hrp study. *Exp. Brain Res.* **63**, 421–430.

Cowan, J. & Friedman, A. 1990 Development and regeneration of eye-brain maps: a computational model. In *Advances in neural information processing systems* (ed. R. Lippman, J. Moody & D. Touretzky), vol. 2, pp. 92–99. San Mateo, CA: Morgan Kaufmann.

Cowan, J. & Friedman, A. 1991 Further studies of a model for the development and regeneration of eye–brain maps. In *Advances in neural information processing systems* (ed. R. Lippman, J. Moody & D. Touretzky), vol. 3, pp. 3–10. San Mateo, CA: Morgan Kaufmann.

Drescher, U., Kremoser, C., Handwerker, C., Löschinger, J., Noda, M. & Bonhoeffer, F. 1995 In vitro guidance of retinal ganglion cell axons by gags, a 25 kda tectal protein related to ligands for eph receptor tyrosine kinases. *Cell* **82**, 359–370.

Fawcett, J. & Willshaw, D. 1982 Compound eyes project stripes on the optic tectum in *xenopus*. *Nature* **296**, 350–352.

Fraser, S. & Perkel, D. 1990 Competitive and positional cues in the patterning of nerve connections. *J. Neurobiol.* **21**, 51–72.

Friedman, E. 1993 Computer simulations of retinotectal maps in goldfish. Ph.D. thesis, University of Chicago, Department of Biophysics and Theoretical Biology.

Friedman, G. & O'Leary, D. 1996 Retroviral misexpression of engrailed genes in the chick optic tectum perturbs the topographic targeting of retinal axons. *J. Neurosci.* **16**, 5498–5509.

Gaze, R. & Sharma, S. 1970 Axial differences in the reinnervation of the goldfish optic tectum by regenerating optic nerve fibres. *Exp. Brain Res.* **10**, 171–181.

Gierer, A. 1983 Model for the retino-tectal projection. *Proc. R. Soc. Lond.* B **218**, 77–93.

Goodman, C. & Shatz, C. 1993 Developmental mecha-

nisms that generate precise patterns of neural connectivity. *Cell Suppl.* **72**, 77–98.

Hayes, W. & Meyer, R. 1988 Optic synapse number but not density is constrained during regeneration onto surgically halved tectum in goldfish: Hrp-em evidence that optic fibres compete for fixed numbers of postsynaptic sites on the tectum. *J. Comp. Neurol.* **274**, 539–59.

Hebb, D. 1949 *The organisation of behaviour*. New York: Wiley.

Holt, C. & Harris, W. 1993 Position, guidance and mapping in the developing visual system. *J. Neurobiol.* **24**, 1400–1422.

Hope, R., Hammond, B. & Gaze, R. 1976 The arrow model: retinotectal specificity and map formation in the goldfish visual system. *Proc. R. Soc. Lond.* B **194**, 447–466.

Horder, T. 1971 Retention, by fish optic nerve fibres regenerating to new terminal sites in the tectum, of 'chemospecific' affinity for their original sites. *J. Physiol. Lond.* **216**, 53P–55P.

Hunt, R. 1976 Position dependent differentiation of neurons. In *Developmental biology* (ed. D. McMahon & C. Fox), pp. 227–256. Menlo Park, CA: Benjamin.

Itasaki, N. & Nakamura, H. 1996 A role for gradient en expression in positional specification on the optic tectum. *Neuron* **16**, 55–62.

Linsker, R. 1986 From basic network principles to neural architecture: emergence of orientation selective cells. *Proc. Natn. Acad. Sci. USA* **83**, 8390–8394.

Linsker, R. 1986 From basic network principles to neural architecture: emergence of orientation columns. *Proc. Natn. Acad. Sci. USA* **83**, 8779–8783.

Linsker, R. 1986 From basic network principles to neural architecture: emergence of spatial opponent cells. *Proc. Natn. Acad. Sci. USA* **83**, 7508–7512.

McLoon, S. 1991 A monoclonal antibody that distinguishes between temporal and nasal retinal axons. *J. Neurosci.* **11**, 1470–1477.

Meyer, R. 1979*a* Retinotectal projection in goldfish to an inappropriate region with a reversal in polarity. *Science* **205**, 819–821.

Meyer, R. 1979*b* 'Extra' optic fibres exclude normal fibres from tectal regions in goldfish. *J. Comp. Neurol.* **183**, 883.

Meyer, R. 1982 Tetrodotoxin blocks the formation of ocular dominance columns in goldfish. *Science* **218**, 589.

Miller, K. 1994 A model for the development of simple cell receptive fields and the ordered arrangement of orientation columns through activity-dependent competition between on- and off-center inputs. *J. Neurosci.* **14**, 409–441.

Miller, K., Keller, J. & Stryker, M. 1989 Ocular dominance column development: analysis and simulation. *Science* **245**, 605–615.

Murray, M., Sharma, S. & Edwards, M. 1982 Target regulation of synaptic number in the compressed retinotectal projection of goldfish. *J. Comp. Neurol.* **209**, 374–385.

Nusslein-Volhard, C. 1994 Of flies and fishes. *Science* **266**, 572–574.

Olson, M. & Meyer, R. 1994 Activity-dependent retinotopic refinement in a low-density retinotectal projection in the goldfish: evidence favouring synaptic cooperation over competition. *J. Neurosci.* **14**, 208–218.

Overton, K. & Arbib, M. 1982 The extended branch–arrow model for the formation of retino-tectal connections. *Biol. Cybern.* **45**, 157–175.

Overton, K. & Arbib, M. 1982 Systems matching and topographic maps: the branch-arrow model. In *Competition and cooperation in neural nets* (ed. S. Amari & M. Arbib), pp. 202–225. Berlin: Springer.

Piepenbrock, C., Ritter, H. & Obermayer, K. 1996 Linear correlation-based learning models require a two-stage process for the development of orientation and ocular dominance. *Neural Processing Lett.* **3**, 31–37.

Piepenbrock, C., Ritter, H. & Obermayer, K. 1997 The joint development of orientation and ocular dominance: role of constraints. *Neural Comp.* **9**, 959–970.

Press, W. H. 1988 *Numerical recipes in C*. Cambridge University Press.

Prestige, M. & Willshaw, D. 1975 On a role for competition in the formation of patterned neural connexions. *Proc. R. Soc. Lond.* B **190**, 77–98.

Raper, J. & Grunewald, E. 1990 Temporal retinal growth cones collapse on contact with nasal retinal axons. *Exp. Neurol.* **109**, 70–74.

Schmidt, J. 1978 Retinal fibres alter tectal positional markers during the expansion of the half retinal projection in goldfish. *J. Comp. Neurol.* **177**, 279–300.

Schmidt, J. & Buzzard, M. 1993 Activity-driven sharpening of the retinotectal projection in goldfish: development under stroboscopic illumination prevents sharpening. *J. Neurobiol.* **24**, 384–399.

Schmidt, J., Cicerone, C. & Easter, S. 1978 Expansion of the half retinal projection to the tectum in goldfish: an electrophysiological and anatomical study. *J. Comp. Neur.* **177**, 257–278.

Sharma, S. 1972 Reformation of retinotectal projections after various tectal ablations in adult goldfish. *Exp. Neurol.* **34**, 171–182.

Sperry, R. 1943 Visuomotor co-ordination in the newt (*triturus viridescens*) after regeneration of the optic nerve. *J. Comp. Neurol.* **79**, 33–55.

Sperry, R. 1963 Chemoaffinity in the orderly growth of nerve fibre patterns and connections. *Proc. Natn. Acad. Sci. USA* **50**, 703–710.

Stahl, B., von Boxberg, Y., Müller, B., Walter, J., Schwartz, U. & Bonhoeffer, F. 1990 Directional cues for retinal axons. *Cold Spring Harbor Symp. Quant. Biol.* **55**, 351–357.

Stetter, M., Müller, A. & Lang, E. W. 1994 Neural network model for the coordinated formation of orientation preference and orientation selectivity maps. *Phys. Rev.* E **50**, 4167–4181.

Straznicky, K. 1978 The acquisition of tectal positional specification in *xenopus*. *Neuroscience Lett.* **9**, 177–184.

Stuermer, C. 1986 Pathways of regenerated retinotectal axons in goldfish. I. optic nerve, tract and tectal fascicle layer. *J. Embryol. Exp. Morphol.* **93**, 1–28.

Stuermer, C. 1988 Trajectories of regenerating retinal axons in the goldfish tectum. I. a comparison of normal and regenerated axons at late regeneration stages. *J. Comp. Neurol.* **267**, 55–68.

Stuermer, C. 1988 Trajectories of regenerating retinal axons in the goldfish tectum. II. exploratory branches and growth cones on axons at early regeneration stages. *J. Comp. Neurol.* **267**, 69–91.

Vielmetter, J., Walter, J. & Stuermer, C. 1991 Regenerating retinal axons of goldfish respond to a repellent guiding component on caudal tectal membranes of adult fish and embryonic chick. *J. Comp. Neurol.* **311**, 321–329.

Walter, J., Henke-Fahle, S. & Bonhoeffer, F. 1987 Avoidance of posterior tectal membranes by temporal retinal

axons. *Development* **101**, 909–913.

Walter, J., Kern-Veits, B., Huf, J., Stolze, B. & Bonhoeffer, F. 1987 Recognition of position-specific properties of tectal cell membranes by retinal axons in vitro. *Development* **101**, 685–696.

Whitelaw, V. & Cowan, J. 1981 Specificity and plasticity of retinotectal connections: a computational model. *J. Neurosci.* **1**, 1369–1387.

Willshaw, D. & von der Malsburg, C. 1979 A marker induction mechanism for the establishment of ordered neural mappings: its application to the retino-tectal problem. *Phil. Trans. R. Soc. Lond.* B **287**, 203–243.

Yoon, M. 1973 Retention of the original topographic polarity by the 180° rotated tectal reimplant in young adult goldfish. *J. Physiol.* **233**, 575–588.

Yoon, M. 1975 Readjustment of retinotectal projection following reimplantation of a rotated or inverted tectal tissue in adult goldfish. *J. Physiol.* **252**, 137–158.

Yoon, M. 1976 Progress of topographic regulation of the visual projection in the halved optic tectum of adult goldfish. *J. Physiol.* **257**, 621–643.

*Received 31 October 1996; accpeted 3 March 1997*